PERGAMON

International Journal of Solids and Structures 38 (2001) 6751–6786

INTERNATIONAL JOURNAL OF SOLIDS and STRUCTURES

www.elsevier.com/locate/ijsolstr

Optimized fiber prestress for reduction of free edge stresses in composite laminates

Alexander P. Suvorov, George J. Dvorak *

Department of Mechanical Engineering, Aeronautical Engineering and Mechanics, Rensselaer Polytechnic Institute, Troy, NY 12180 3590, USA

Received 28 August 2000; in revised form 12 April 2001

Abstract

An analytical procedure is described for evaluation of the effect of release of fiber prestress, applied prior to matrix consolidation, on stress distribution in individual plies and at free edges of laminated composite plates. Both thermal changes, piecewise uniform transformation strains in the plies and overall mechanical loads can be considered in the analysis. The thermal and transformation load contributions are decomposed into superpositions of certain uniform fields with mechanical loads. Release of fiber prestress is regarded as an equivalent uniaxial compression applied at the edges of each prestressed ply. Optimized distributions of fiber prestress are found in individual plies such that stresses in both laminate interior and at the free edges remain within allowable limits, while the applied mechanical load may change from zero to a certain maximum value. Specific results are found for cross-ply and quasi-isotropic symmetric S-glass/epoxy laminates under tension. They clearly demonstrate the substantial potential of fiber prestress in damage control and prevention in laminated composite structures.

Keywords: Composite laminates; Fiber prestress; Free edge stresses; Optimized prestress distribution; Ply strength limits; Damage envelope

1. Introduction

Few problems in mechanics of composites have attracted such long lasting attention as analysis of interlaminar stresses at free edges of laminate plates. The early work was initiated by Hayashi (1967), and much advanced by Pipes and Pagano (1970), Pagano (1978a,b), and Wang and Choi (1982). The variational approach to free edge problems, suggested by Pagano (1978a,b), is based on Reissner's (1950) variational principle. It is capable of satisfying traction and displacement continuity conditions at interfaces between adjacent layers, and also stress equilibrium in the sense of vanishing resultant force and moment in separate sub-regions, normally chosen as layers of the laminate. More recent results, based on

* Corresponding author. Tel.: +1-518-276-6940; fax: +1-518-276-8784.
E-mail address: dvorak@rpi.edu (G.J. Dvorak).

0020-7683/01/$ - see front matter
PII: S0020-7683(01)00106-8

minimizing the complementary energy, are obtained using statically admissible fields that satisfy stress equilibrium and traction continuity conditions pointwise but do not satisfy displacement continuity conditions across layer interfaces. They have been developed, primarily for uniaxial tension and cylindrical bending, by Kassapoglou and Lagace (1986), Rose and Herakovich (1993), Yin (1994a,b), Flanagan (1994), Kim and Atluri (1995a,b), and Cho and Kim (2000). More accurate solution methods for stress fields in the entire laminate under general loading have been recently proposed by Vel and Batra (2000) and Wang et al. (2000). Several attempts have been made at using the analytical results in improving laminate design, mainly by selecting laminate stacking sequences and/or layups that reduce the interlaminar stress magnitudes. Some of these are reviewed by Herakovich (1998). Among the most notable is the discovery by Christensen and DeTeresa (1992) of nearly zero interlaminar stresses in the quasi-isotropic $(0/\pm 60)$ laminates loaded by remotely applied tension in the 0° direction. This layup, with minor deviations from the ± 60 angles, offers the said advantages in many laminate systems, providing that the tensile load is applied only in the 0°, $+60$ or -60 directions (Alberski, 2000). Kim and Atluri (1995a,b) have examined a different methodology for reducing the free edge stresses. They found optimal through-thickness temperature gradients that when applied together with uniaxial loading completely eliminate or minimize the interlaminar stresses.

The present work explores a new method of reducing the free edge stresses, by applying an optimized prestress to the fibers in selected plies prior to matrix consolidation, and releasing this prestress after matrix cure. The prestress magnitudes needed in most applications are well within the capability of present equipment used in filament winding or fiber placement fabrication procedures (Table 1) and are often applied in reducing fiber waviness for improvement of ply compressive strength. Related uses of fiber prestress in residual stress reductions in cylindrical shells have been examined in our recent work (Dvorak et al., 1999; Srinivas et al., 1999). Applications to damage control in laminates have been explored by Dvorak and Suvorov (2000).

The loads applied to the laminate in the present work include not only mechanical loading by normal stresses and bending and twisting moments, but also thermal strains and other eigenstrains or transformation strains that may be applied in individual plies, and of course, release of fiber prestress at the free edges. Section 2 presents various definitions and certain decomposition procedures that convert the transformation strain loads into uniform fields and equivalent mechanical loads. Section 3 outlines a simple application of this approach to reduction and/or complete elimination of thermal residual stresses caused by cooling from fabrication temperatures. Section 4 reviews the boundary conditions of the problems considered and the solution method used, based in part on Yin's (1994a,b) implementation of the minimum complementary energy principle. Section 5 outlines the optimization procedure for evaluation of ply prestress distribution under prescribed loads, subject to constraints derived from laminate strength criteria. Section 6 presents many results illustrating the potential of fiber prestress in reducing both free edge stresses and improving resistance to matrix cracking in the interior sections of several laminates.

Table 1
Force needed to generate 1000 MPa stress in filaments/tow

Fiber	Diameter (μm)	Filaments/tow	Force (N)
S-glass	14	2000	307.88
S-glass	6	2000	56.54
Kevlar	12	1000	113.12
Carbon AS4	8	12000	603.19
Carbon IM8	5	12000	235.64
Carbon P-100S	10	2000	157.08
Nicalon (SiC)	15	500	88.35

2. Problem formulation

2.1. Geometry, material properties and loading

The laminated plate considered here consists of a certain number N of thin fibrous layers or plies bonded at $n = N - 1$ parallel plane interfaces. Fig. 1 shows schematically a representative volume element in the (X, Y, Z) global or overall coordinate system where the in-plane dimensions $-a < X < a$, $-b < Y < b$ are assumed much larger than the total thickness, a, $b \gg t$. The X-axis coincides with the fiber direction in the 0° plies and the Z-axis with the out-of-plane direction. The plies $i = 1, 2, \ldots, N$ are numbered starting from the bottom of the plate; interfaces between plies are numbered in the same order, with $Z = z_{i-1}$ denoting the lower interface of the ith layer, and $Z = z_0$ the bottom surface of the laminate. The fiber direction in each ply i coincides with the x_1^i-axis of the local (x_1^i, x_2^i, x_3^i) coordinate system, where x_3^i is parallel to Z. The angle ϕ_i is measured counterclockwise from the laminate 0° or X-direction to the fiber direction x_1^i in the ith ply. Ply thickness is denoted by t_i and the thickness of the laminate by $t = \sum t_i$.

The individual layers are regarded as homogeneous and at most orthotropic in the local system, with one plane of material symmetry parallel to the plane of the plate, and one aligned with the direction of the fiber axis in each ply. Elastic compliance and stiffness of each ply are first estimated in the local coordinate system (x_1^i, x_2^i, x_3^i) by one of several available methods. The ply constitutive relations are then written in the local and overall coordinate systems as

$$\boldsymbol{\epsilon}_i = \boldsymbol{S}_i \boldsymbol{\sigma}_i + \boldsymbol{\alpha}_i \Delta\theta + \boldsymbol{\mu}_i, \tag{1a}$$

$$\bar{\boldsymbol{\epsilon}}_i = \bar{\boldsymbol{S}}_i \bar{\boldsymbol{\sigma}}_i + \bar{\boldsymbol{\alpha}}_i \Delta\theta + \bar{\boldsymbol{\mu}}_i \tag{1b}$$

where, in the local coordinates (x_1^i, x_2^i, x_3^i), the $\boldsymbol{\epsilon}_i$ and $\boldsymbol{\sigma}_i$ are the (6×1) ply strain and stress fields, $\boldsymbol{S}_i$ is the (6×6) ply compliance matrix, $\Delta\theta$ is a uniform change in temperature. The $\boldsymbol{\alpha}_i = \{\alpha_1^i \ \alpha_2^i \ \alpha_3^i \ 0 \ 0 \ 0\}^{\mathrm{T}}$ is the vector of linear thermal expansion coefficients of the ply, and $\boldsymbol{\mu}_i = \{\mu_1^i \ \mu_2^i \ \mu_3^i \ 0 \ 0 \ \mu_6^i\}^{\mathrm{T}}$ is a vector of ply transformation strains or eigenstrains.

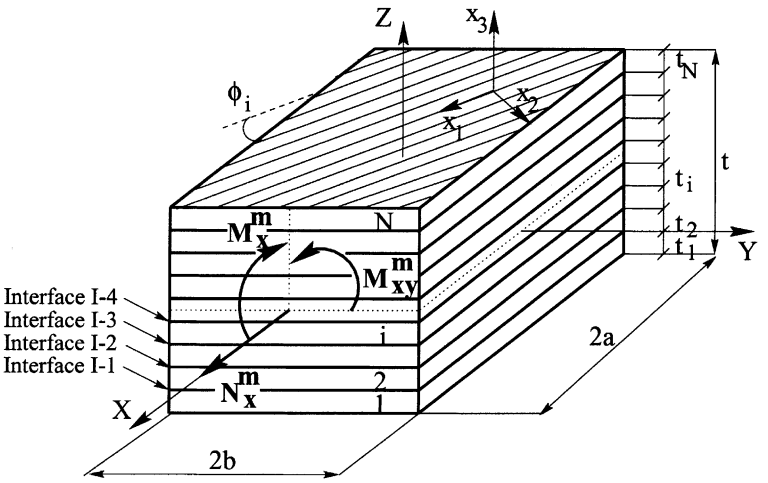

Fig. 1. Geometry of an element of a laminated plate.

The terms in Eq. (1a) transform into the overall (X, Y, Z) coordinates according to

$$\bar{\boldsymbol{\epsilon}}_i = \boldsymbol{T}_i^{\mathrm{T}} \boldsymbol{\epsilon}_i, \quad \bar{\boldsymbol{\sigma}}_i = \boldsymbol{R}_i^{\mathrm{T}} \boldsymbol{\sigma}_i, \quad \bar{\boldsymbol{S}}_i = \boldsymbol{T}_i^{\mathrm{T}} \boldsymbol{S}_i \boldsymbol{T}_i \tag{2}$$

The $\boldsymbol{S}$, $\boldsymbol{R}$ and $\boldsymbol{T}$ matrices are described in Appendix A. The $\boldsymbol{\alpha}_i$ and $\boldsymbol{\mu}_i$ transform as strain tensors. After this transformation, the nonzero coefficients of the compliance and stiffness matrices coincide with those of a monoclinic system.

The applied loads considered in the present analysis include: (i) Thermal strains and other transformation strains or eigenstrains that appear in Eq. (1a). These are stress-free deformations that a ply would experience if free of constraints. In addition to phase transformations, moisture absorption, inelastic deformation, as well as certain equivalent eigenstrains can be regarded as transformation strains. (ii) Uniform normal and shear tractions applied at the free edges $X = \pm a$ or $Y = \pm b$ of individual plies, e.g., by release of fiber prestress. (iii) Uniform average in-plane tractions, as well as bending and twisting moments, attached to the laminate at locations far removed from that of the representative element in Fig. 1; these can be contributed both by actual mechanical loads and by force and moment resultants of free edge tractions applied in solving for the above loads (i) and of the tractions simulating release of fiber prestress (ii).

Regardless of their origin, each of the above load systems is assumed to create an interior stress field in the laminate, far away from the free edges, that depends only on the thickness coordinate Z and not on the in-plane XY-coordinates. The interior stress and deformation fields can be obtained by a laminated plate theory; these have been described by Christensen (1979), Whitney (1988), Noor and Burton (1989) and Reddy (1997), among others.

Both top and bottom surfaces of the laminate are assumed to be traction free. The tractions applied at the free edges are uniform in the X- or Y-directions, respectively, so that the free edge stress fields are functions of the YZ- or XZ-coordinates, and thus need to be evaluated only on planes $X = 0$ and/or $Y = 0$ in Fig. 1, far away from the corners of the representative volume element.

2.2. Decomposition of transformation fields

The effect of uniform thermal changes and other ply eigenstrains on the residual stresses in the plies is modeled by a superposition of certain uniform equivalent tractions applied at ply free edges, with a piecewise uniform stress field in the laminate.

Consider a laminated plate of any layup, separate the plies, and let each ply be subjected to uniform, stress-free transformation strains given by Eq. (1a) at $\boldsymbol{\sigma}_i = \boldsymbol{0}$. In general, these strains are different in each ply, so the laminate cannot be reassembled; however, the plies remain plane and parallel to each other. Next, attach auxiliary in-plane tractions at all free edges of each ply to generate in-plane ply stresses $\hat{\boldsymbol{\sigma}}_i$, that in superposition with the local transformation strains create the following uniform in-plane strains in each ply

$$\begin{aligned} \hat{\epsilon}_1^i &= S_{11}^i \hat{\sigma}_1^i + S_{12}^i \hat{\sigma}_2^i + \alpha_1^i \Delta\theta + \mu_1^i, \\ \hat{\epsilon}_2^i &= S_{12}^i \hat{\sigma}_1^i + S_{22}^i \hat{\sigma}_2^i + \alpha_2^i \Delta\theta + \mu_2^i, \\ \hat{\epsilon}_6^i &= S_{66}^i \hat{\sigma}_6^i + \mu_6^i \end{aligned} \tag{3}$$

The auxiliary tractions can be selected to make the total ply strains isotropic in the $x_1^i x_2^i$-plane and of the same magnitude in all plies

$$\hat{\epsilon}_1^i = \hat{\epsilon}_2^i = \hat{\epsilon}, \quad \hat{\epsilon}_6^i = 0 \tag{4}$$

This yields the magnitudes of the auxiliary stresses,

$$\hat{\sigma}_1^i = \frac{S_{22}^i(\hat{\epsilon} - \alpha_1^i \Delta\theta - \mu_1^i) - S_{12}^i(\hat{\epsilon} - \alpha_2^i \Delta\theta - \mu_2^i)}{S_{11}^i S_{22}^i - S_{12}^{i2}},$$

$$\hat{\sigma}_2^i = \frac{S_{11}^i(\hat{\epsilon} - \alpha_2^i \Delta\theta - \mu_2^i) - S_{12}^i(\hat{\epsilon} - \alpha_1^i \Delta\theta - \mu_1^i)}{S_{11}^i S_{22}^i - S_{12}^{i2}}, \tag{5}$$

$$\hat{\sigma}_6^i = -\frac{\mu_6^i}{S_{66}^i}$$

The uniform, isotropic in-plane strain $\hat{\epsilon}$ is a constant that can be selected at will. A convenient choice is $\hat{\epsilon} = 0$, which renders the stresses (5) equal to the eigenstresses caused in each ply by the applied eigenstrains. Since the in-plane ply strains are now of the same magnitude in all plies, the laminate can be reassembled. Finally, the auxiliary in-plane tractions that support the uniform strain state in the presence of ply eigenstrains need to be removed. The auxiliary stress vectors are transformed from the local coordinates of the ith ply to the global (X, Y, Z) coordinates, Fig. 2, and applied with reversed signs as surface tractions at the respective ply edges. The ply unloading vectors are defined as,

$$-\bar{\hat{\boldsymbol{\sigma}}}_i = -\boldsymbol{R}_i^{\mathrm{T}}\{\hat{\sigma}_1^i \ \hat{\sigma}_2^i \ 0 \ 0 \ 0 \ \hat{\sigma}_6^i\}^{\mathrm{T}} \tag{6}$$

The final residual stress state in the laminate is obtained by superimposing the uniform ply stresses (5) with those generated by the force and moment resultants of the ply vectors (6). These may cause bending and twisting in other than symmetric and symmetrically loaded laminates. The final residual strain state is found by superimposing the uniform strain field (4) with that caused in the laminate by the unloading vectors (6). Clearly, no free edge stress concentrations are associated with the uniform strains (4), which include the applied ply eigenstrains. Such concentrations are caused only by the purely mechanical unloading (6), and can thus be analyzed using available procedures.

Thermal and other normal transformation strain components can also be specified in the x_3-direction. In the context of Eq. (3), the out-of-plane strains are,

$$\hat{\epsilon}_3^i = S_{31}^i \hat{\sigma}_1^i + S_{32}^i \hat{\sigma}_2^i + \alpha_3^i \Delta\theta + \mu_3^i, \quad \hat{\epsilon}_4^i = \hat{\epsilon}_5^i = 0 \tag{7}$$

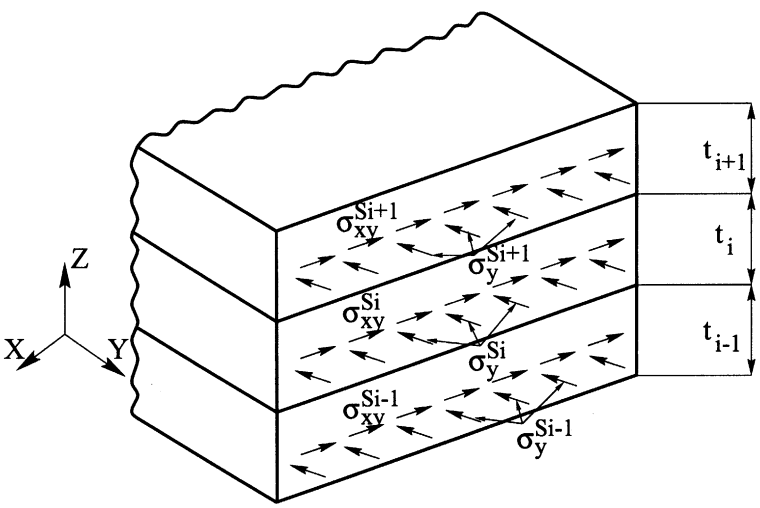

Fig. 2. Free edge $Y = b$ loaded with equivalent tractions.

The overall through-the-thickness strain associated with the auxiliary uniform in-plane strain state is obtained as $\hat{\epsilon}_3 = \sum(t_i/t)\hat{\epsilon}_3^i$, where t_i and t are the ply and laminate thicknesses, respectively. Superposition of Eq. (7) with the strains caused by Eq. (6) provides the final magnitudes. In laminates loaded by compressive stresses normal to their plane, the resulting in-plane ply deformations can be regarded as additional eigenstrains (Dvorak and Suvorov, 2000, Section 5).

2.3. Free edge tractions representing release of fiber prestress

Fiber prestress $(\sigma_{11}^f)_P^i$ is defined as the average stress applied to the fiber prior to solidification of the matrix. As in *op. cit.*, the average in-plane ply tractions that support the fiber prestress after fabrication and processing are specified in the local coordinates of each ply as

$$\boldsymbol{\sigma}_f^{pi} = \{c_f^i(\sigma_{11}^f)_P^i \; 0 \; 0 \; 0 \; 0 \; 0\}^{\mathrm{T}} \tag{8}$$

where c_f^i is the fiber volume fraction. Release of fiber prestress can be regarded, on average, as application of uniform ply free edge tractions that cancel Eq. (8) at the edges. After transformation to the global coordinates (Fig. 2) the nonzero components become

$$\begin{aligned} -\sigma_x^{pi} &= -c_f^i(\sigma_{11}^f)_P^i \cos^2(\phi_i), \\ -\sigma_y^{pi} &= -c_f^i(\sigma_{11}^f)_P^i \sin^2(\phi_i), \\ -\sigma_{xy}^{pi} &= -c_f^i(\sigma_{11}^f)_P^i \cos(\phi_i)\sin(\phi_i) \end{aligned} \tag{9}$$

where ϕ_i is the angle that the ith ply fiber direction contains with the X-axis.

Together, the piecewise uniform ply traction distributions (6) and (9) specify the boundary conditions in solutions of problems involving ply thermal and other transformation strains, and release of fiber prestress. The uniform fields (3) and (4) represent a part of such solutions.

3. Thermal stress reduction by fiber prestress

A simple and potentially useful application of fiber prestress can be made in laminates which are subjected to large residual stresses after fabrication or in service. With certain exceptions noted below, a distribution of fiber prestress in individual plies can be found such that it reduces to zero the free edge residual stress field caused by fixed thermal and possibly other transformation strains induced by cooling from a fabrication temperature.

As an example, consider a laminated plate of any layup that is subjected to a uniform thermal change $\Delta\theta$ applied during cooling from the fabrication temperature. In-plane moduli and thermal expansion coefficients of all plies need to be identical, and as is the case in most composites, the expansion coefficient of the matrix is assumed to be larger than that of the fiber, hence during cooling a free ply contracts more in the transverse direction. In turn, the prestress release contributes to a positive transverse strain and compressive longitudinal strain. This allows application of fiber prestress that creates the same isotropic strain field in all plies, and thus cancels the thermal stress concentrations at the free edges of the laminate.

To evaluate the required prestress magnitude, the decomposition procedure outlined in Section 2.2 is used again – the plies are separated, and each ply is subjected to the uniform, stress-free thermal strain. In general, these strains are different in the plane of each ply, so the laminate cannot be reassembled. Next, suppose that a certain fiber prestress $\hat{\sigma}_1 = -c_f(\sigma_{11}^f)_P$ has been released. The prestress magnitude is selected such that after its release, and in superposition with the thermal strain, an isotropic in-plane strain field is created in each ply

$$\hat{\epsilon} = S_{11}\hat{\sigma}_1 + \alpha_1 \Delta\theta = S_{12}\hat{\sigma}_1 + \alpha_2 \Delta\theta \tag{10}$$

The required prestress value in each ply is thus found as

$$(\sigma_{11}^f)_P = \frac{(\alpha_2 - \alpha_1)\Delta\theta}{c_f(S_{12} - S_{11})} > 0 \tag{11}$$

and the uniform strain in all plies after cooling and prestress release as

$$\hat{\epsilon} = [(S_{12}\alpha_1 - S_{11}\alpha_2)\Delta\theta]/(S_{12} - S_{11}) \tag{12}$$

Note that, according to Eq. (A.1), $(S_{11} - S_{12}) = (1 + \nu_{12})/E_1 > 0$, the assumption is that $\alpha_2 - \alpha_1 > 0$ and $\Delta\theta < 0$. Since all plies are deformed by the same isotropic in-plane strain, and are free of tractions, the laminate can be reassembled. The strain (12) is preserved through laminate thickness. Note that neither this strain nor the prestress (11) depend on ply orientation or laminate layup. Of course, local concentrations at the free fiber ends are not eliminated by the prestress.

4. Solution method

4.1. Interior fields and free edge boundary conditions

In standard free edge problems, the boundary conditions typically prescribe zero surface tractions at one pair of free edges, such as the planes $Y = \pm b$ in Fig. 1, and an average normal strain, together with a bending moment and torque at the other pair, $X = \pm a$. In the present case, the boundary conditions must also reflect the presence of equivalent tractions generated by ply transformation fields and prestress release. These are represented by a piecewise uniform distribution of ply surface tractions applied at the lateral planes $X = \pm a$ and $Y = \pm b$ in Fig. 1. With reference to Eqs. (2), (5) and (9), after transformation to the overall coordinates, these ply tractions will be denoted as

$$\bar{\boldsymbol{\sigma}}^{si} = -\boldsymbol{R}_i^{\mathrm{T}}[\hat{\boldsymbol{\sigma}}_i + \boldsymbol{\sigma}^{pi}] = \{\sigma_x^{si}\ \sigma_y^{si}\ 0\ 0\ 0\ \sigma_{xy}^{si}\}^{\mathrm{T}} \tag{13}$$

where $\bar{\boldsymbol{\sigma}}^{si}$ are the total free edge tractions applied to the ith ply, defined in the overall (X, Y, Z) system (Fig. 2). The $\hat{\boldsymbol{\sigma}}_i$ are the equivalent tractions (5) and (6), and the $-\boldsymbol{\sigma}^{pi}$ are ply tractions caused by prestress release (9), and $\boldsymbol{R}_i^{\mathrm{T}}$ is the coordinate transformation matrix introduced in Eq. (2).

The tractions (13) generate both free edge and interior fields in the laminate, the latter are superimposed with the uniform fields (3), (4) and (12), transformed into the overall system, and with the fields induced by any actual mechanical loading. The interior fields that will be denoted by $\tilde{\boldsymbol{\sigma}}$ can be found by a lamination plate theory. In constructing this solution, it is convenient to decompose the total load applied to the laminate of Fig. 1 into two subsystems, #1 that is applied only at $X = \pm a$ while the edges $Y = \pm b$ are traction free, and subsystem #2 applied at $Y = \pm b$ while the other pair of edges is traction free. In both subsystems, there are no tractions at the top and bottom surface of the laminate.

Let the #1 subsystem consist of both the equivalent ply loads (13) present at $X = \pm a$, and actually applied mechanical loads denoted by superscript (m), so that the total force and moment resultants become,

$$\begin{aligned} N_x^{(1)} &= \int_{z_0}^{z_N} \sigma_x^{si(1)}\,\mathrm{d}Z + N_x^m, \quad M_x^{(1)} = \int_{z_0}^{z_N} \sigma_x^{si(1)} Z\,\mathrm{d}Z + M_x^m, \\ N_{xy}^{(1)} &= \int_{z_0}^{z_N} \sigma_{xy}^{si(1)}\,\mathrm{d}Z + N_{xy}^m, \quad M_{xy}^{(1)} = \int_{z_0}^{z_N} \sigma_{xy}^{si(1)} Z\,\mathrm{d}Z + M_{xy}^m \end{aligned} \tag{14}$$

For the corresponding interior stress field to be independent of the X-coordinate, and for the displacements to be continuous across ply interfaces, the displacements in all plies must represent generalized plane deformation of the form (Lekhnitskii, 1963),

$$\begin{aligned} u^{(1)} &= (A_1 Y - B_1 Z + C_1)X + U_1(Y,Z) + \omega_1 Z - \omega_2 Y + u_0^{(1)}, \\ v^{(1)} &= -A_1 X^2/2 - \Theta_1 XZ + V_1(Y,Z) + \omega_2 X - \omega_3 Z + v_0^{(1)}, \\ w^{(1)} &= B_1 X^2/2 + \Theta_1 XY + W_1(Y,Z) + \omega_3 Y - \omega_1 X + w_0^{(1)} \end{aligned} \tag{15}$$

where the constants A_1 and B_1 describe uniform bending with respect to the Z and Y axes, and C_1, Θ_1 uniform extension and rotation with respect to the X-axis. The functions $V_1(Y,Z)$ and $W_1(Y,Z)$ represent in-plane deformations, $U_1(Y,Z)$ characterizes the warping of the plane of the cross-section $X = \text{const}$, while the ω_1–ω_3 and $u_0^{(1)}$, $v_0^{(1)}$, $w_0^{(1)}$ are parts of the rigid body displacements. For example, the strains and bending and twisting curvatures of the plate, predicted by the classical laminated plate theory for the #1 loading subsystems (14) are,

$$\epsilon_y^{(1)} = \epsilon_y^0 - Z\kappa_y^0, \quad \epsilon_x^{(1)} = C_1 - B_1 Z, \quad \gamma_{xy}^{(1)} = \gamma_{xy}^0 - \Theta_1 Z \tag{16}$$

Since the edges $Y = \pm b$ are traction free under the #1 subsystem, the constants ϵ_y^0, γ_{xy}^0, and κ_y^0 are chosen such that, in sections removed from the loaded ends, the resultants of the interior fields,

$$\begin{aligned} N_y^{(1)} &= \int_{z_0}^{z_N} \tilde{\sigma}_y^{(1)}\,\mathrm{d}Z = 0, \quad M_y^{(1)} = \int_{z_0}^{z_N} \tilde{\sigma}_y^{(1)} Z\,\mathrm{d}Z = 0, \\ N_{yx}^{(1)} &= \int_{z_0}^{z_N} \tilde{\sigma}_{yx}^{(1)}\,\mathrm{d}Z = 0, \quad M_{yx}^{(1)} = \int_{z_0}^{z_N} \tilde{\sigma}_{yx}^{(1)} Z\,\mathrm{d}Z = 0 \end{aligned} \tag{17}$$

The subsystem #2 represents only the equivalent tractions (13) applied at the edges $Y = \pm b$, which are free of any mechanical loads. The interior stress and strain fields caused by this loading are the same as those caused in an extended laminate by the resultants,

$$\begin{aligned} N_y^{(2)} &= \int_{z_0}^{z_N} \sigma_y^{si(2)}\,\mathrm{d}Z, \quad M_y^{(2)} = \int_{z_0}^{z_N} \sigma_y^{si(2)} Z\,\mathrm{d}Z, \\ N_{yx}^{(2)} &= \int_{z_0}^{z_N} \sigma_{yx}^{si(2)}\,\mathrm{d}Z, \quad M_{yx}^{(2)} = \int_{z_0}^{z_N} \sigma_{yx}^{si(2)} Z\,\mathrm{d}Z \end{aligned} \tag{18}$$

The displacement field follows from Eq. (15) by changing the X-axis components to Y-axis components, and vice versa. Similar changes are required in Eq. (16), which now becomes,

$$\epsilon_x^{(2)} = \epsilon_x^0 - Z\kappa_x^0, \quad \epsilon_y^{(2)} = C_2 - B_2 Z, \quad \gamma_{yx}^{(2)} = \gamma_{yx}^0 - \Theta_2 Z \tag{19}$$

The constants ϵ_x^0, γ_{yx}^0 and κ_x^0 are again chosen such that in sections removed from the loaded ends, the resultants on $X = \pm a$ are,

$$\begin{aligned} N_x^{(2)} &= \int_{z_0}^{z_N} \tilde{\sigma}_x^{(2)}\,\mathrm{d}Z = 0, \quad M_x^{(2)} = \int_{z_0}^{z_N} \tilde{\sigma}_x^{(2)} Z\,\mathrm{d}Z = 0, \\ N_{xy}^{(2)} &= \int_{z_0}^{z_N} \tilde{\sigma}_{xy}^{(2)}\,\mathrm{d}Z = 0, \quad M_{xy}^{(2)} = \int_{z_0}^{z_N} \tilde{\sigma}_{xy}^{(2)} Z\,\mathrm{d}Z = 0 \end{aligned} \tag{20}$$

Additional conditions connecting the shear force resultants are presented in Appendix B.

On planes $X = 0$ at $-b \ll Y \ll +b$, and $Y = 0$ at $-a \ll X \ll +a$, that are removed from the free and mechanically loaded edges of the laminate, the interior stress and deformation fields generated by the two above subsystems are functions of only the Z-coordinate. Collectively, they will be denoted by,

$$\tilde{\boldsymbol{\sigma}}^i = \tilde{\boldsymbol{\sigma}}_i^{(1)} + \tilde{\boldsymbol{\sigma}}_i^{(2)} = \{\tilde{\sigma}_x^i\ \tilde{\sigma}_y^i\ \tilde{\sigma}_z^i\ \tilde{\sigma}_{yz}^i\ \tilde{\sigma}_{xz}^i\ \tilde{\sigma}_{xy}^i\}^{\mathrm{T}},$$
$$\tilde{\boldsymbol{\epsilon}}^i = \tilde{\boldsymbol{\epsilon}}_i^{(1)} + \tilde{\boldsymbol{\epsilon}}_i^{(2)} = \{\tilde{\epsilon}_x^i\ \tilde{\epsilon}_y^i\ \tilde{\epsilon}_z^i\ \tilde{\epsilon}_{yz}^i\ \tilde{\epsilon}_{xz}^i\ \tilde{\epsilon}_{xy}^i\}^{\mathrm{T}} \tag{21}$$

With reference to Figs. 1 and 2, the problem at hand can be formulated as follows: For a prescribed average normal strain, bending moment and torque at the edges $X = \pm a$, find the stress field in the cross-section $X = 0$ of the laminate, under the free edge and interior boundary conditions prescribed through the thickness of each ply $i = 1, 2, \ldots, N$,

$$\begin{aligned}
&\sigma_y^i = \sigma_y^{si} \text{ at } Y = \pm b, \quad \sigma_y^i \to \tilde{\sigma}_y^i \text{ at } Y \to 0,\\
&\sigma_{xy}^i = \sigma_{xy}^{si} \text{ at } Y = \pm b, \quad \sigma_{xy}^i \to \tilde{\sigma}_{xy}^i \text{ at } Y \to 0,\\
&\sigma_{yz}^i = 0 \text{ at } Y = \pm b, \quad \sigma_{yz}^i \to 0 \text{ at } Y \to 0
\end{aligned} \tag{22}$$

such that it satisfies traction continuity conditions at ply interfaces $Z = z_i$

$$\begin{aligned}
&\sigma_{xz}^i = \sigma_{xz}^{i+1},\\
&\sigma_{yz}^i = \sigma_{yz}^{i+1},\\
&\sigma_z^i = \sigma_z^{i+1}
\end{aligned} \tag{23}$$

and zero traction conditions on laminate surface planes $Z = z_0, z_N$

$$\begin{aligned}
&\sigma_{xz}^1|_{Z=z_0} = \sigma_{yz}^1|_{Z=z_0} = \sigma_z^1|_{Z=z_0} = 0,\\
&\sigma_{xz}^N|_{Z=z_N} = \sigma_{yz}^N|_{Z=z_N} = \sigma_z^N|_{Z=z_N} = 0,
\end{aligned} \tag{24}$$

The above boundary and interface conditions must conform with the overall equilibrium conditions. For piecewise uniform tractions boundary conditions at $Y = 0$ and $Y = \pm b$ the equilibrium conditions can be formulated as

$$\int_{Y=0}^{Y=b} \sigma_{yz}^j|_{Z=z_j}\,\mathrm{d}Y + \sum_{i=1}^{j}[\sigma_y^{si} - \tilde{\sigma}_y^i]t_i = 0 \tag{25}$$

$$\int_{Y=0}^{Y=b} \sigma_z^j|_{Z=z_j} Y\,\mathrm{d}Y + \sum_{i=1}^{j}[\sigma_y^{si} - \tilde{\sigma}_y^i]t_i\left[-\frac{t_i}{2} + \sum_{k=i}^{j} t_k\right] = 0 \tag{26}$$

$$\int_{Y=0}^{Y=b} \sigma_{xz}^j|_{Z=z_j}\,\mathrm{d}Y + \sum_{i=1}^{j}[\sigma_{xy}^{si} - \tilde{\sigma}_{xy}^i]t_i = 0 \tag{27}$$

4.2. Admissible stress fields

The stresses in the $X = 0$ plane of each ith layer of the laminated plate can now be represented by a pair of stress functions $F^i(Y,Z)$ and $\Psi^i(Y,Z)$ (Lekhnitskii, 1963), such that,

$$\begin{aligned}
&\sigma_y^i = F_{,zz}^i, \quad \sigma_z^i = F_{,yy}^i, \quad \sigma_{yz}^i = -F_{,yz}^i,\\
&\sigma_{xz} = -\Psi_{,y}^i, \quad \sigma_{xy} = \Psi_{,z}^i
\end{aligned} \tag{28}$$

The remaining stress σ_x^i is determined from,

$$\sigma_x^i = \frac{1}{\bar{S}_{11}^i}(\epsilon_x^i - \{\bar{S}_{12}^i\sigma_y^i + \bar{S}_{13}^i\sigma_z^i + \bar{S}_{16}^i\sigma_{xy}^i\}) \tag{29}$$

where $\bar{\boldsymbol{S}}$ is the ply compliance in the overall coordinate system as in Eq. (2) and ϵ_x^i is the normal strain in the ith ply. In Eq. (29) we assumed that the axial normal strain ϵ_x^i is uniform in the Y-direction, and thus a function of only the Z-coordinate, determined by the selected lamination theory solution for the interior field. For example, for the loading subsystems #1 and #2, this strain is given as

$$\epsilon_x^i = C - BZ, \quad z_{i-1} \leqslant Z \leqslant z_i \tag{30}$$

where C is the axial strain in X-direction of the plane $Z = 0$ and B is the curvature characterizing bending deformation with respect to the Y-axis.

Next, we adopt the polynomial approximations of the stress functions suggested by Yin (1994a,b),

$$F^i(Y,\eta) = (1 - 3\eta^2 + 2\eta^3)F_{i-1}(Y) + (\eta - 2\eta^2 + \eta^3)t_i G_{i-1}(Y) + (3\eta^2 - 2\eta^3)F_i(Y) + (\eta^3 - \eta^2)t_i G_i(Y)$$
$$i = 1, 2, \ldots, N \tag{31}$$

$$\Psi^i(Y,\eta) = (1 - \eta^2)\Psi_{i-1}(Y) + \eta^2\Psi_i(Y) + (\eta - \eta^2)t_i H_{i-1}(Y) \tag{32}$$

where the nondimensional thickness coordinate

$$\eta = (Z - z_{i-1})/(z_i - z_{i-1}), \quad i = 1, 2, \ldots, N \tag{33}$$

The $F_i(Y)$ and $F_{i-1}(Y)$ are values of $F^i(Y,Z)$ on the interfaces $Z = z_i$ and $Z = z_i - 1$ and the Z-derivative of the function takes values $G_i(Y)$ and $G_{i-1}(Y)$ on these interfaces. Similarly, $\Psi_i(Y)$ is the value of $\Psi^i(Y,Z)$ on the ith interface $Z = z_i$ and $H_i(Y)$ is the value of the Z-derivative of the function on the upper side of the ith interface. The stress fields represented by Eqs. (31) and (32) can be shown to comply with the interface traction continuity conditions (23).

As noted by Yin (1994a,b), the present polynomial approximation of the stress functions admits linear through the ply thickness distribution of in-plane stresses σ_y^i and σ_{xy}^i. Thus, the order of a given approximation is sufficient to allow application of piecewise uniform distributions of ply tractions σ_y^{si} and σ_{xy}^{si} caused by ply transformation fields and release of prestress and also of interior stress fields linear through ply thickness. Selection of higher order polynomials would provide for even higher order stress distributions. It is worth noting that the stress functions (31) and (32) do not produce a stress singularity at the free edge $Y = \pm b$. It was found by Ye (1990) that the singular orders of interlaminar stress expansions at the free edge are at least by 10 times smaller than $-1/2$, and hence, the strength of the singularity is quite weak. Nevertheless, the presence of singularity can be manifested by higher order polynomial expansions of the stress functions F^i and Ψ^i in the thickness coordinate. For example, solutions based on quintic polynomial expansions of F^i and cubic expansions of Ψ^i produced steeper stress gradients near the free edge (Yin, 1994a,b) than those obtained from the stress functions (31) and (32). Since the objective function (61) introduced later for solving optimization problem does not include interlaminar stress components, the present polynomial approximation of stress functions given by Eqs. (31) and (32) without singular terms appears to be sufficiently accurate.

Boundary conditions for the functions F_i, F_i' G_i, G_i', Ψ_i, H_i at the free edges $Y = \pm b$ and at $Y = 0$ follow from Eq. (22). The required stresses found from Eq. (28) to Eq. (32) are

$$\sigma_y^i = \frac{1}{t_i^2}[(-6 + 12\eta)F_{i-1}(Y) + (-4 + 6\eta)t_i G_{i-1}(Y) + (6 - 12\eta)F_i(Y) + (6\eta - 2)t_i G_i(Y)],$$
$$\sigma_{yz}^i = -\frac{1}{t_i}[(-6\eta + 6\eta^2)F_{i-1}'(Y) + (1 - 4\eta + 3\eta^2)t_i G_{i-1}'(Y) + (6\eta - 6\eta^2)F_i'(Y) + (3\eta^2 - 2\eta)t_i G_i'(Y)],$$
$$\sigma_{xy}^i = \frac{1}{t_i}[-2\eta\Psi_{i-1}(Y) + 2\eta\Psi_i(Y) + (1 - 2\eta)t_i H_{i-1}(Y)] \tag{34}$$

Then, using Eq. (22) one can derive at $Y = b$ and $Y = 0$,

$$\begin{aligned}
&\frac{1}{t_i^2}[-6F_{i-1}(b) - 4t_iG_{i-1}(b) + 6F_i(b) - 2t_iG_i(b)] = \sigma_y^{si}|_{Z=z_{i-1}}\\
&\frac{1}{t_i^2}[6F_{i-1}(b) + 2t_iG_{i-1}(b) - 6F_i(b) + 4t_iG_i(b)] = \sigma_y^{si}|_{Z=z_i}\\
&\frac{1}{t_i^2}[-6F_{i-1}(0) - 4t_iG_{i-1}(0) + 6F_i(0) - 2t_iG_i(0)] = \tilde{\sigma}_y^{i}|_{Z=z_{i-1}}\\
&\frac{1}{t_i^2}[6F_{i-1}(0) + 2t_iG_{i-1}(0) - 6F_i(0) + 4t_iG_i(0)] = \tilde{\sigma}_y^{i}|_{Z=z_i} \quad i = 1,2,\ldots,N
\end{aligned} \tag{35}$$

$$\begin{aligned}
&H_{i-1}(b) = \sigma_{xy}^{si}|_{Z=z_{i-1}},\\
&\frac{1}{t_i}[-2\Psi_{i-1}(b) + 2\Psi_i(b) - t_iH_{i-1}(b)] = \sigma_{xy}^{si}|_{Z=z_i},\\
&H_{i-1}(0) = \tilde{\sigma}_{xy}^{i}|_{Z=z_{i-1}},\\
&\frac{1}{t_i}[-2\Psi_{i-1}(0) + 2\Psi_i(0) - t_iH_{i-1}(0)] = \tilde{\sigma}_{xy}^{i}|_{Z=z_i} \quad i = 1,2,\ldots,N
\end{aligned} \tag{36}$$

$$\begin{aligned}
&F_i'(b) = G_i'(b) = 0,\\
&F_i'(0) = G_i'(0) = 0 \quad i = 1,2,\ldots,N
\end{aligned} \tag{37}$$

Values of the stress functions at the bottom and top surfaces of the laminate can be found by enforcing equilibrium conditions. Force equilibrium in the Y-direction implies

$$N_y = \sum_{i=1}^{N}\int_{z_{i-1}}^{z_i}\sigma_y^i\,\mathrm{d}Z = \sum_{i=1}^{N}\int_{z_{i-1}}^{z_i}F_{,zz}^i\,\mathrm{d}Z = \sum_{i=1}^{N}F_{,z}^i|_{z_{i-1}}^{z_i} = -G_0 + G_N \tag{38}$$

where the subscripts 0 and N identify values of the bottom and top laminate planes, respectively. Moment equilibrium with respect to X-axis requires

$$\begin{aligned}
M_y &= \sum_{i=1}^{N}\int_{z_{i-1}}^{z_i}\sigma_y^iZ\,\mathrm{d}Z = \sum_{i=1}^{N}\int_{z_{i-1}}^{z_i}F_{,zz}^iZ\,\mathrm{d}Z = \sum_{i=1}^{N}F_{,z}^iZ|_{z_{i-1}}^{z_i} - \sum_{i=1}^{N}F^i|_{z_{i-1}}^{z_i}\\
&= (-F_N + G_Nz_N) + (F_0 - G_0z_0)
\end{aligned} \tag{39}$$

Force equilibrium in the X-direction requires

$$N_{yx} = \sum_{i=1}^{N}\int_{z_{i-1}}^{z_i}\sigma_{xy}^i\,\mathrm{d}Z = \sum_{i=1}^{N}\int_{z_{i-1}}^{z_i}\Psi_{,z}^i\,\mathrm{d}Z = \sum_{i=1}^{N}\Psi^i|_{z_{i-1}}^{z_i} = -\Psi_0 + \Psi_N \tag{40}$$

The absence of surface tractions at the top and bottom surfaces of the plate (24) implies that G_0, G_N, Ψ_0 and Ψ_N are constants and F_0, F_N are at most linear functions of Y. However, because the bending moment in Eq. (39) is constant, F_0, F_N should be chosen as constants as well.

Without loss of generality, the stress functions in the first ply at the bottom surface of the laminate can be selected to satisfy

$$F_0 = G_0 = \Psi_0 = 0 \tag{41}$$

Then, from Eqs. (38)–(40), one can find the following values at the top surface of the laminate

$$G_N = N_y, \quad F_N = N_y z_N - M_y, \quad \Psi_N = N_{yx} \tag{42}$$

According to the definition of $H_i(Y)$ in Eq. (32) the function $H_N = 0$.

The remaining ply stress functions to be found are $F_1(Y)$, $F_2(Y)$, …, $F_n(Y)$, $G_1(Y)$, $G_2(Y)$, …, $G_n(Y)$, $\Psi_1(Y)$, $\Psi_2(Y)$, …, $\Psi_n(Y)$, and $H_0(Y)$, $H_1(Y)$, …, $H_n(Y)$, where $n = N - 1$ is the total number of ply interfaces. Solution of the systems of linear equations (35) and (36) provides for the boundary values of these functions and the values at the top surface F_N, G_N and Ψ_N given in Eq. (42).

4.3. Minimum of the complementary energy functional

Governing equations for the $4n + 1$ stress functions $F_i(Y)$, $G_i(Y)$, $\Psi_i(Y)$ and $H_i(Y)$ defining the admissible field in the laminate are found from a stationary value of the complementary energy functional,

$$U = \frac{1}{2}\int\int \epsilon_{pq}\sigma_{pq}\,\mathrm{d}Y\,\mathrm{d}Z - \int\int_{A_u} \boldsymbol{T}_k^{\mathrm{T}}\bar{\boldsymbol{u}}_k\,\mathrm{d}A \quad pq = x, y, z, yz, xz, xy, \;\; k = 1, 2, 3 \tag{43}$$

where A_u is the area over which displacements $\bar{\boldsymbol{u}}_k$ are prescribed, and $\boldsymbol{T}_k$ is the traction vector corresponding to those displacements.

The displacements in the cross-section $X = \text{const}$ are given as

$$\begin{aligned} u &= (C - BZ)X + U(Y, Z), \\ v &= -\Theta ZX + V(Y, Z), \\ w &= \Theta XY + W(Y, Z) \end{aligned} \tag{44}$$

where $U(Y, Z)$, $V(Y, Z)$ and $W(Y, Z)$ are unknown functions, C is the axial strain in the plane $Z = 0$, B is the bending curvature and Θ is the twisting curvature. The constants C, B, and Θ are obtained from a lamination theory solution for two load systems #1 and #2. Then, the surface integral in the expression for the complementary energy for the element of the laminate of unit length $X^{(1)} - X^{(2)} = 1$ can be written as

$$\int\int_{A_u} \boldsymbol{T}_k^{\mathrm{T}}\bar{\boldsymbol{u}}_k\,\mathrm{d}A = \int_{Z=z_0}^{Z=z_N}\int_{Y=0}^{Y=b} [(C - BZ)\sigma_x^i - \Theta Z\sigma_{xy}^i + \Theta Y\sigma_{xz}^i]\,\mathrm{d}Y\,\mathrm{d}Z \tag{45}$$

Elimination of the longitudinal stress component σ_x^i with the use of Eq. (29) and change of variables (33) lead to the final expression for the complementary energy in terms of stress components (28)

$$\begin{aligned} U = \frac{1}{2}\sum_{i=1}^{N}\int_{\eta=0}^{\eta=1}\int_{Y=0}^{Y=b} \Bigg\{ & \sigma_y^{i2}\bar{\bar{S}}_{22}^i + \sigma_z^{i2}\bar{\bar{S}}_{33}^i + \sigma_{yz}^{i2}\bar{\bar{S}}_{44}^i + \sigma_{xz}^{i2}\bar{\bar{S}}_{55}^i + \sigma_{xy}^{i2}\bar{\bar{S}}_{66}^i + 2\sigma_y^i\sigma_z^i\bar{\bar{S}}_{23}^i + 2\sigma_y^i\sigma_{xy}^i\bar{\bar{S}}_{26}^i + 2\sigma_z^i\sigma_{xy}^i\bar{\bar{S}}_{36}^i \\ & + 2\sigma_{yz}^i\sigma_{xz}^i\bar{\bar{S}}_{45}^i - 2\frac{(C - B(z_{i-1} + \eta t_i))^2}{\bar{S}_{11}^i} + 2(C - B(z_{i-1} + \eta t_i))\left[\frac{\bar{S}_{12}^i}{\bar{S}_{11}^i}\sigma_y^i + \frac{\bar{S}_{13}^i}{\bar{S}_{11}^i}\sigma_z^i + \frac{\bar{S}_{16}^i}{\bar{S}_{11}^i}\sigma_{xy}^i\right] \\ & + 2\Theta(z_{i-1} + \eta t_i)\sigma_{xy}^i - 2\Theta Y\sigma_{xz}^i\Bigg\} t_i\,\mathrm{d}Y\,\mathrm{d}\eta \end{aligned} \tag{46}$$

where,

$$\bar{\bar{S}}_{ij}^i = \bar{S}_{ij}^i - \frac{\bar{S}_{1i}^i\bar{S}_{1j}^i}{\bar{S}_{11}^i}, \quad i, j = 2, 3, \ldots, 6 \tag{47}$$

The stationary value of the complementary energy functional is equated to zero,

$$\delta U = 0 \tag{48}$$

Substitution of stresses (28), expressed in terms of stress functions (31) and (32), into Eq. (48), integration first with respect to η, and then by parts with respect to Y, yields a system of $4n+1$ ordinary differential equations for the $4n+1$ unknown functions $F_i(Y)$, $G_i(Y)$, $\Psi_i(Y)$ and $H_i(Y)$.

Let the functions $F_i(Y)$, $G_i(Y)$, $\Psi_i(Y)$, $i=1, 2, \ldots, n$ and $H_i(Y)$, $i=0, 1, \ldots, n$ be arranged as components of $(n\times 1)$ vectors $\boldsymbol{F}$, $\boldsymbol{G}$, $\boldsymbol{\Psi}$ and $(n+1\times 1)$ vector $\boldsymbol{H}$, respectively,

$$\begin{aligned}
\boldsymbol{F} &= \{F_1(Y)F_2(Y)\ldots F_n(Y)\}^{\mathrm{T}}\\
\boldsymbol{G} &= \{G_1(Y)G_2(Y)\ldots G_n(Y)\}^{\mathrm{T}}\\
\boldsymbol{\Psi} &= \{\Psi_1(Y)\Psi_2(Y)\ldots \Psi_n(Y)\}^{\mathrm{T}}\\
\boldsymbol{H} &= \{H_0(Y)H_1(Y)\ldots H_n(Y)\}^{\mathrm{T}}
\end{aligned} \tag{49}$$

In turn, define column vector $\boldsymbol{X}$ as,

$$\boldsymbol{X} = \{\boldsymbol{F}^{\mathrm{T}}\ \boldsymbol{G}^{\mathrm{T}}\ \boldsymbol{\Psi}^{\mathrm{T}}\ \boldsymbol{H}^{\mathrm{T}}\}^{\mathrm{T}} \tag{50}$$

Then the system of ordinary differential equations can be conveniently written as,

$$\boldsymbol{W}\boldsymbol{X}^{IV} + \boldsymbol{V}\boldsymbol{X}^{II} + \boldsymbol{U} = \boldsymbol{b}(C, B, \Theta, N_y, M_y, N_{xy}) \tag{51}$$

where $\boldsymbol{W}$, $\boldsymbol{V}$ and $\boldsymbol{U}$ are $(4n+1)\times(4n+1)$ constant real symmetric matrices, and $\boldsymbol{b}$ is a $4n+1\times 1$ constant vector depending on axial strain in X-direction C, bending curvature with respect to Y-axis B, twisting curvature Θ, in-plane normal stress resultant along Y-axis N_y, bending moment with respect to X-axis M_y and shearing stress resultant N_{xy}. Note that a single component from each of the following pairs of variables is prescribed on the boundary of the laminated plate,

$$\epsilon_x N_x,\ \ \epsilon_y N_y,\ \ \gamma_{xy} N_{xy},\ \ k_x M_x,\ \ k_y M_y,\ \ \Theta M_{xy} \tag{52}$$

A particular solution of Eq. (51) is chosen to be a constant vector,

$$\boldsymbol{X}^p = \boldsymbol{U}^{-1}\boldsymbol{b} \tag{53}$$

This corresponds to the interior stress fields $\tilde{\boldsymbol{\sigma}}$ Eq. (21), found with the help of a lamination theory, for the laminate subjected to deformation characterized by three constants C, B and Θ, and traction boundary conditions characterized by force resultants N_y, N_{xy} and moment resultant M_y. This implies that

$$\begin{aligned}
&F_i^p = F_i(0),\ \ G_i^p = G_i(0),\ \ \Psi_i^p = \Psi_i(0), \quad i = 1, 2, \ldots, n,\\
&H_i^p = H_i(0), \quad i = 0, 1, 2, \ldots, n
\end{aligned} \tag{54}$$

where $F_i(0)$, $G_i(0)$, $\Psi_i(0)$ and $H_i(0)$ are found by solving Eqs. (35) and (36).

The homogeneous solution to Eq. (51) is sought in the following form

$$\begin{aligned}
&\boldsymbol{F} = \boldsymbol{p}^F \exp(\omega(b-Y)), \quad \boldsymbol{G} = \boldsymbol{p}^G \exp(\omega(b-Y)),\\
&\Psi = \boldsymbol{p}^\Psi \exp(\omega(b-Y)), \quad \boldsymbol{H} = \boldsymbol{p}^H \exp(\omega(b-Y))
\end{aligned} \tag{55}$$

where $\boldsymbol{p}^F$, $\boldsymbol{p}^G$, $\boldsymbol{p}^\Psi$, $\boldsymbol{p}^H$ are yet unknown constant vectors. According to Eq. (54) the homogeneous solution (55) should vanish away from the free edges at $Y=0$. Define,

$$\boldsymbol{p} = \{\boldsymbol{p}^{F^{\mathrm{T}}}\ \boldsymbol{p}^{G^{\mathrm{T}}}\ \boldsymbol{p}^{\Psi^{\mathrm{T}}}\boldsymbol{p}^{H^{\mathrm{T}}}\}^{\mathrm{T}} \tag{56}$$

Substitution of Eq. (55) into the homogeneous part of Eq. (51) reduces the differential equations to the system of algebraic equations

$$\omega^4 \boldsymbol{W}\boldsymbol{p} + \omega^2 \boldsymbol{V}\boldsymbol{p} + \boldsymbol{U}\boldsymbol{p} = 0 \tag{57}$$

Solution of the eigenvalue problem (57) yields $12n + 2$ eigenvalues ω. Details of the solution are presented in Appendix C. Only values of ω with negative real part should be left in the solution (55) so that the interlaminar stresses decay in the interior region of laminate. Therefore, only $6n + 1$ eigenvalues ω are selected and the homogeneous solution is obtained by a linear combination of $6n + 1$ eigenvectors,

$$\begin{aligned} F_i^H &= p_{ij}^F s_j \exp(\omega_j(b - Y)), \\ G_i^H &= p_{ij}^G s_j \exp(\omega_j(b - Y)), \\ \Psi_i^H &= p_{ij}^\Psi s_j \exp(\omega_j(b - Y)), \quad i = 1, 2, \ldots, n, \ \ j = 1, 2, \ldots, 6n + 1, \\ H_i^H &= p_{ij}^H s_j \exp(\omega_j(b - Y)), \quad i = 0, 1, \ldots, n, \ \ j = 1, 2, \ldots, 6n + 1 \end{aligned} \tag{58}$$

where s_j are constants to be determined. The total solution is a sum of homogeneous (58) and particular (54) solutions

$$\begin{aligned} F_i &= p_{ij}^F s_j \exp(\omega_j(b - Y)) + F_i^p, \\ G_i &= p_{ij}^G s_j \exp(\omega_j(b - Y)) + G_i^p, \\ \Psi_i &= p_{ij}^\Psi s_j \exp(\omega_j(b - Y)) + \Psi_i^p, \quad i = 1, 2, \ldots, n, \ \ j = 1, 2, \ldots, 6n + 1, \\ H_i &= p_{ij}^H s_j \exp(\omega_j(b - Y)) + H_i^p, \quad i = 0, 1, \ldots, n, \ \ j = 1, 2, \ldots, 6n + 1 \end{aligned} \tag{59}$$

The $6n + 1$ constants s_j are determined from $6n + 1$ boundary conditions by prescribing $F_i(b)$, $G_i(b)$, $F_i'(b)$, $G_i'(b)$, $\Psi_i(b)$, $i = 1, 2, \ldots, n$ and $H_i(b)$, $i = 0, 1, \ldots, n$ from Eqs. (35)–(37). In view of Eq. (54), the traction boundary conditions at the interior of the laminate $Y = 0$ are satisfied provided that $\exp(\omega_j b)$ is of negligible magnitude.

This completes solution of the problem. The stress field in each layer can be found from Eqs. (28) and (29). The interlaminar stress along the ith interface may be obtained directly as,

$$\begin{aligned} \sigma_z &= F_i''(Y) \\ \sigma_{yz} &= -G_i'(Y) \\ \sigma_{xz} &= -\Psi_i'(Y) \quad i = 1, 2, \ldots, n \end{aligned} \tag{60}$$

5. Optimized fiber prestress distribution

5.1. Objective function and constraints

Here we examine the use of fiber prestress for reduction of the total free edge stress components that contribute to specific failure modes at ply interfaces. In particular, the peel stress σ_z promotes mode I fracture, and the shears σ_{xz} and σ_{yz} may induce modes II and III along the edges $X = \pm a$. At $Y = \pm b$, the σ_{xz} and σ_{yz} contribute to modes III and II. An algorithm will be developed that allows selection of a specific fiber prestress distribution in individual plies such that a certain objective function of the total free edge stresses at $Y = \pm b$ is minimized. Several forms of the objective function can be employed, involving either the above local stresses, or the in-plane surface tractions at ply free edges, or both. In the absence of experimental data that would support a specific selection, we have explored functions minimizing the maxima or averages of interfacial stress components, but found them less effective in providing stable solutions than those that minimize the differences between the in-plane interior and surface stress components. In particular, due to highly nonuniform interlaminar stress distribution along the interfaces the stress maxima are reached at a priori unknown points generally different for each interface and stress component. On the other hand, definition of interlaminar stress averages, such as the one proposed by Brewer and Lagace

(1988) for their delamination criterion, requires the selection of averaging distance. Ambiguity that exists in both approaches reduces chances of cancellation of free edge stresses and leads to complications in the formulation. Since the present stress-reduction method is based on application of free edge tractions by prestress release, we seek prestress magnitudes that minimize the objective function,

$$I = \sum_{i=1}^{N}[(\sigma_y^{si,p} - \tilde{\sigma}_y^{i,p}) + (\sigma_y^{si,m} - \tilde{\sigma}_y^{i,m}) + (\sigma_y^{si,\theta} - \tilde{\sigma}_y^{i,\theta})]^2 + [(\sigma_{xy}^{si,p} - \tilde{\sigma}_{xy}^{i,p}) + (\sigma_{xy}^{si,m} - \tilde{\sigma}_{xy}^{i,m}) + (\sigma_{xy}^{si,\theta} - \tilde{\sigma}_{xy}^{i,\theta})]^2 \to \min \tag{61}$$

where $i = 1, 2, \ldots, N$ is the ply number and the superscripts m, θ and p denote, respectively, certain in-plane stress components caused by mechanical, ply thermal eigenstrains $\boldsymbol{\alpha}_j \Delta\theta$, and prestress loads. The stresses $\sigma_y^{si,p}$, $\sigma_y^{si,m}$, $\sigma_y^{si,\theta}$, and $\sigma_{xy}^{si,p}$, $\sigma_{xy}^{si,m}$, $\sigma_{xy}^{si,\theta}$ are the surface tractions at $Y = b$, the stresses denoted by letters with a tilde are ply stresses at $Y = 0$, found by a lamination theory, caused either by mechanical loads N_x, M_x, M_{xy} applied at the edges $X = \pm a$ or surface tractions $\sigma_y^{si,p}$, $\sigma_y^{si,\theta}$, and $\sigma_{xy}^{si,p}$, $\sigma_{xy}^{si,\theta}$ applied at the free edges $Y = \pm b$. The surface tractions at the free edges $Y = \pm b$, caused by mechanical loads applied at $X = \pm a$ are zeros, i.e., $\sigma_y^{si,m} = \sigma_{xy}^{si,m} = 0$. The equivalent surface tractions generated by ply thermal eigenstrains and prestress release are given by Eq. (13).

Denoting $\sigma_{pq}^{i,\alpha} + \sigma_{pq}^{i,\beta} = \sigma_{pq}^{i,\alpha\beta}$, Eq. (61) can be expanded as

$$\begin{aligned} I = {} & \sum_{i=1}^{N}(\sigma_y^{si,p})^2 + (\tilde{\sigma}_y^{i,p})^2 - 2\sigma_y^{si,p}\tilde{\sigma}_y^{i,p} + (\sigma_{xy}^{si,p})^2 + (\tilde{\sigma}_{xy}^{i,p})^2 - 2\sigma_{xy}^{si,p}\tilde{\sigma}_{xy}^{i,p} + (\sigma_y^{si,m\theta})^2 + (\tilde{\sigma}_y^{i,m\theta})^2 - 2\sigma_y^{si,m\theta}\tilde{\sigma}_y^{i,m\theta} \\ & + (\sigma_{xy}^{si,m\theta})^2 + (\tilde{\sigma}_{xy}^{i,m\theta})^2 - 2\sigma_{xy}^{si,m\theta}\tilde{\sigma}_{xy}^{i,m\theta} + 2\{\sigma_y^{si,p}\sigma_y^{si,m\theta} + \tilde{\sigma}_y^{i,p}\tilde{\sigma}_y^{i,m\theta} - \tilde{\sigma}_y^{i,p}\sigma_y^{si,m\theta} - \tilde{\sigma}_y^{i,m\theta}\sigma_y^{si,p}\} \\ & + 2\{\sigma_{xy}^{si,p}\sigma_{xy}^{si,m\theta} + \tilde{\sigma}_{xy}^{i,p}\tilde{\sigma}_{xy}^{i,m\theta} - \tilde{\sigma}_{xy}^{i,p}\sigma_{xy}^{si,m\theta} - \tilde{\sigma}_{xy}^{i,m\theta}\sigma_{xy}^{si,p}\} \to \min \end{aligned} \tag{62}$$

Assuming that applied loads are fixed, the terms that do not include $\sigma_{pq}^{si,p}$ and $\tilde{\sigma}_{pq}^{i,p}$ are constant and can be excluded from the objective function; this provides

$$\begin{aligned} I = {} & \sum_{i=1}^{N}(\sigma_y^{si,p})^2 + (\tilde{\sigma}_y^{i,p})^2 - 2\sigma_y^{si,p}\tilde{\sigma}_y^{i,p} + (\sigma_{xy}^{si,p})^2 + (\tilde{\sigma}_{xy}^{i,p})^2 - 2\sigma_{xy}^{si,p}\tilde{\sigma}_{xy}^{i,p} + 2\{\sigma_y^{si,p}\sigma_y^{si,m\theta} + \tilde{\sigma}_y^{i,p}\tilde{\sigma}_y^{i,m\theta} \\ & - \tilde{\sigma}_y^{i,p}\sigma_y^{si,m\theta} - \tilde{\sigma}_y^{i,m\theta}\sigma_y^{si,p}\} + 2\{\sigma_{xy}^{si,p}\sigma_{xy}^{si,m\theta} + \tilde{\sigma}_{xy}^{i,p}\tilde{\sigma}_{xy}^{i,m\theta} - \tilde{\sigma}_{xy}^{i,p}\sigma_{xy}^{si,m\theta} - \tilde{\sigma}_{xy}^{i,m\theta}\sigma_{xy}^{si,p}\} \to \min \end{aligned} \tag{63}$$

Although the interlaminar stresses are not initially included in Eq. (61), they need to be reflected in the constraints that assure that the local stresses do not violate prescribed failure criteria anywhere in the laminate; this leads to the form (73) and constraints (74)–(76) below. Since these stresses are not uniform, their computed magnitudes can be sampled at selected distances from the free edges. For example, along the free edge $Y = b$, the sampling points can be chosen at positions $Y = b - t_i/l$, with $l = \infty$, 6, 4, 3, 2, 1 and t_i denoting the thickness of the ith ply. Similar positions can be selected along all free edges. Our numerical tests showed that these points are sufficient to capture or approximate well the interfacial stress maxima. At each interface k, magnitudes of the thermal (θ), thermomechanical ($m\theta$) and prestress-induced (p) interfacial stress components found at the above l – distances can be assembled in vectors,

$$\sigma_{pq}^{k,\theta} = (\boldsymbol{r}_{pq}^{l})_k, \quad \sigma_{pq}^{k,m\theta} = (\boldsymbol{g}_{pq}^{l})_k, \quad pq = z, yz, xz, \quad l = \infty, 6, 4, 3, 2, 1, \quad Y = b - t_i/l \tag{64}$$

$$\sigma_{pq}^{k,p} = (\boldsymbol{Q}_{pq}^{l})_{ki}(\boldsymbol{P})_i \quad i = 1, 2, \ldots, N \;\; k = 1, 2, \ldots, n, \quad Y = b - t_i/l \tag{65}$$

$$\boldsymbol{P} = [(\sigma_{11}^{f})_P^1 \; (\sigma_{11}^{f})_P^2 \cdots (\sigma_{11}^{f})_P^N]^{\mathrm{T}} \tag{66}$$

where the $(n \times N)$ influence matrices $(\boldsymbol{Q}_{pq}^{l})_{ki}$ consist of coefficients that are values of the $\sigma_{pq}^{k,p}$ stress components caused at the kth interface at $Y = b - t_i/l$ by a unit prestress applied to the ith ply.

Analogously, the in-plane stress components (13) and the in-plane average ply stresses (21) can be assembled in vectors

$$\sigma_{pq}^{sj,m\theta} = (\boldsymbol{q}_{pq})_j, \quad pq = y, xy, \;\; j = 1, 2, \ldots, N \tag{67}$$

$$(\tilde{\sigma}_{pq}^{j,m\theta}) = (\tilde{\boldsymbol{q}}_{pq})_j \tag{68}$$

$$\sigma_{pq}^{sj,p} = (\boldsymbol{Q}_{pq}^S)_{ji}(\boldsymbol{P})_i, \quad pq = y, xy, \;\; i, j = 1, 2, \ldots, N \tag{69}$$

$$\tilde{\sigma}_{pq}^{j,p} = (\tilde{\boldsymbol{Q}}_{pq})_{ji}(\boldsymbol{P})_i, \quad pq = y, xy, \;\; i, j = 1, 2, \ldots, N \tag{70}$$

Using these relations, one can write Eq. (63) as

$$\begin{aligned} I = {} & (\boldsymbol{P})_j\{(\boldsymbol{Q}_y^S)_{jk}(\boldsymbol{Q}_y^S)_{ki} + (\tilde{\boldsymbol{Q}}_y)_{jk}(\tilde{\boldsymbol{Q}}_y)_{ki} - (\boldsymbol{Q}_y^S)_{jk}(\tilde{\boldsymbol{Q}}_y)_{ki} - (\tilde{\boldsymbol{Q}}_y)_{jk}(\boldsymbol{Q}_y^S)_{ki} + (\boldsymbol{Q}_{xy}^S)_{jk}(\boldsymbol{Q}_{xy}^S)_{ki} + (\tilde{\boldsymbol{Q}}_{xy})_{jk}(\tilde{\boldsymbol{Q}}_{xy})_{ki} \\ & - (\boldsymbol{Q}_{xy}^S)_{jk}(\tilde{\boldsymbol{Q}}_{xy})_{ki} - (\tilde{\boldsymbol{Q}}_{xy})_{jk}(\boldsymbol{Q}_{xy}^S)_{ki}\}(\boldsymbol{P})_i + 2\{(\boldsymbol{q}_y)_k(\boldsymbol{Q}_y^S)_{ki} + (\tilde{\boldsymbol{q}}_y)_k(\tilde{\boldsymbol{Q}}_y)_{ki} - (\boldsymbol{q}_y)_k(\tilde{\boldsymbol{Q}}_y)_{ki} - (\tilde{\boldsymbol{q}}_y)_k(\boldsymbol{Q}_y^S)_{ki} \\ & + (\boldsymbol{q}_{xy})_k(\boldsymbol{Q}_{xy}^S)_{ki} + (\tilde{\boldsymbol{q}}_{xy})_k(\tilde{\boldsymbol{Q}}_{xy})_{ki} - (\boldsymbol{q}_{xy})_k(\tilde{\boldsymbol{Q}}_{xy})_{ki} - (\tilde{\boldsymbol{q}}_{xy})_k(\boldsymbol{Q}_{xy}^S)_{ki}\}(\boldsymbol{P})_i \to \min \end{aligned} \tag{71}$$

Defining,

$$\begin{aligned} \boldsymbol{Q}_{ji} = {} & (\boldsymbol{Q}_y^S)_{jk}(\boldsymbol{Q}_y^S)_{ki} + (\tilde{\boldsymbol{Q}}_y)_{jk}(\tilde{\boldsymbol{Q}}_y)_{ki} - (\boldsymbol{Q}_y^S)_{jk}(\tilde{\boldsymbol{Q}}_y)_{ki} - (\tilde{\boldsymbol{Q}}_y)_{jk}(\boldsymbol{Q}_y^S)_{ki} + (\boldsymbol{Q}_{xy}^S)_{jk}(\boldsymbol{Q}_{xy}^S)_{ki} \\ & + (\tilde{\boldsymbol{Q}}_{xy})_{jk}(\tilde{\boldsymbol{Q}}_{xy})_{ki} - (\boldsymbol{Q}_{xy}^S)_{jk}(\tilde{\boldsymbol{Q}}_{xy})_{ki} - (\tilde{\boldsymbol{Q}}_{xy})_{jk}(\boldsymbol{Q}_{xy}^S)_{ki}, \\ f_i = {} & \{(\boldsymbol{q}_y)_k(\boldsymbol{Q}_y^S)_{ki} + (\tilde{\boldsymbol{q}}_y)_k(\tilde{\boldsymbol{Q}}_y)_{ki} - (\boldsymbol{q}_y)_k(\tilde{\boldsymbol{Q}}_y)_{ki} - (\tilde{\boldsymbol{q}}_y)_k(\boldsymbol{Q}_y^S)_{ki}\} + \{(\boldsymbol{q}_{xy})_k(\boldsymbol{Q}_{xy}^S)_{ki} \\ & + (\tilde{\boldsymbol{q}}_{xy})_k(\tilde{\boldsymbol{Q}}_{xy})_{ki} - (\boldsymbol{q}_{xy})_k(\tilde{\boldsymbol{Q}}_{xy})_{ki} - (\tilde{\boldsymbol{q}}_{xy})_k(\boldsymbol{Q}_{xy}^S)_{ki}\} \end{aligned} \tag{72}$$

and dividing Eq. (71) by 2 one can write the objective function in the standard form,

$$I = \frac{1}{2}(\boldsymbol{P})_j\boldsymbol{Q}_{ji}(\boldsymbol{P})_i + f_i(\boldsymbol{P})_i \to \min \tag{73}$$

Denote the ply strength limits as follows. Let $F_1^{t,c} > 0$, $F_2^{t,c} > 0$ be axial and transverse ply strength in tension (t) or compression (c), and $F_6 > 0$ – the strength in shear. The fiber strength is defined as $F_f^t = F_1^t/c_f$.

The optimization problem (73) is accompanied by the following constraints. Since only tensile forces may be applied such that the fiber strength F_t^f is not exceeded, we require that

$$0 \leqslant (\boldsymbol{P})_i \leqslant F_f^t, \quad i = 1, 2, \ldots, N \tag{74}$$

Moreover, the interlaminar stresses caused at the interfaces by application of fiber prestress alone and after superposition with the interlaminar stresses caused by the mechanical loads should not exceed applicable ply strength limits. Using the influence matrices (65) one may write the following constraints for the interlaminar stresses resulting from change in temperature and application of fiber prestress,

$$\begin{aligned} & -F_2^c \leqslant (\boldsymbol{r}_z^l)_k + (\boldsymbol{Q}_z^l)_{ki}(\boldsymbol{P})_i \leqslant F_2^t \\ & -F_6 \leqslant (\boldsymbol{r}_{yz}^l)_k + (\boldsymbol{Q}_{yz}^l)_{ki}(\boldsymbol{P})_i \leqslant F_6 \\ & -F_6 \leqslant (\boldsymbol{r}_{xz}^l)_k + (\boldsymbol{Q}_{xz}^l)_{ki}(\boldsymbol{P})_i \leqslant F_6, \quad k = 1, 2, \ldots, n, \;\; l = \infty, 6, 4, 3, 2, 1 \end{aligned} \tag{75}$$

Requiring that the interlaminar stresses, resulting from application of both fiber prestress and thermomechanical loads, do not exceed strength limits, one can write additional inequality constraints,

$$
\begin{aligned}
&-F_2^c \leqslant (\boldsymbol{g}_z^l)_k + (\boldsymbol{Q}_z^l)_{ki}(\boldsymbol{P})_i \leqslant F_2^t \\
&-F_6 \leqslant (\boldsymbol{g}_{yz}^l)_k + (\boldsymbol{Q}_{yz}^l)_{ki}(\boldsymbol{P})_i \leqslant F_6 \\
&-F_6 \leqslant (\boldsymbol{g}_{xz}^l)_k + (\boldsymbol{Q}_{xz}^l)_{ki}(\boldsymbol{P})_i \leqslant F_6, \quad k = 1, 2, \ldots, n, \quad l = \infty, 6, 4, 3, 2, 1
\end{aligned} \tag{76}
$$

We note that similar constraints must be observed by the interior stress fields (21) and (53).

Inclusion of singular terms or higher order polynomial approximation for the stress functions (31) and (32) could result in higher interfacial stress maxima induced by both thermomechanical loads and fiber prestress at the vicinity of the free edges $Y = \pm b$. Free edge solution methods providing the singular terms could be used as sources of the local stresses induced by the mechanical and transformation loads, and by the prestress release in Eqs. (64)–(73), as well as in the constraints (74)–(76). However, the optimized prestress distributions should not change significantly because the increase in the stress maxima caused solely by thermomechanical loading is counteracted by the increase in the stresses caused by release of fiber prestress.

The problem of optimizing the quadratic function (73) subject to linear inequality constraints (74)–(76) is solved by the active set method described by Gill et al. (1991). The solution procedure involves calculation of an initial feasible point and the generation of an iterative sequence of feasible points that converge to the optimal solution. At each iteration, the set of active constraints is updated in that a constraint is either added or removed from the active set. The null space of the active constraints is found and the new search direction is sought that minimizes the objective function in this null space. Maximum feasible steplength is then computed along the search direction and a constraint corresponding to this steplength is included in the active set at the next iteration. However, if the steplength is unity the vector of Lagrange multipliers is evaluated. If all Lagrange multipliers are positive, an optimal solution has been obtained. Otherwise, at the next iteration a constraint that corresponds to the smallest negative Lagrange multiplier is removed from the active set.

The results presented in this paper have been obtained using MATLAB software (version 5.3).

6. Examples

6.1. Material properties, loading and reported results

Specific evaluations of fiber prestress needed to minimize free edge stresses in different loading situations are now presented for two symmetric 9-layer S-glass epoxy laminates, with $((0/90)_2/\bar{0})_s$ and $(0/45/-45/90/\bar{0})_s$ layups. Ply and constituent properties are listed in Tables 2 and 3.

In all laminates, the 0° plies are aligned with the X-axis. The ends $X = \pm a$ of the large laminate element in Fig. 1 are assumed clamped and loaded by prescribed mechanical loads. The free edges are located at $Y = \pm b$. Equivalent tractions representing the unloading Eq. (6) or Eq. (13) are applied at all edges.

Laminates are first subjected to a uniform change in temperature, $\Delta\theta = -150$°C, as they would be during fabrication. For this loading case, we find prestress values that completely eliminate free edge stress concentrations in any layup, and find the interior stress and strain fields in the prestressed laminate. Next, three additional loading situations are examined: (a) Free edge and interior stresses are evaluated for loading of the laminates by the temperature change $\Delta\theta = -150$°C applied together with a tensile force N_x at the $X = \pm a$ edges of the laminate. The force magnitude is chosen to cause a total normal strain in the loading direction corresponding to about 0.75 of the estimated ultimate laminate strain, or less if required by the ply strength criteria (74)–(76). (b) Optimized fiber prestress distribution is evaluated such that its release minimizes the free edge stress concentrations for loading of the laminate by N_x and $\Delta\theta = -150$°C. (c) Finally the free edge and interior stresses determined for the loading cases (a) and (b) are superimposed.

Table 2
Properties of S-glass epoxy ply

Property	
Fiber volume ratio, c_f	0.4461
Longitudinal modulus, E_1 (GPa)	43
Transverse modulus, E_2 (GPa)	8.9
In-plane shear modulus, G_{12} (GPa)	4.5
Major Poisson's ratio, ν_{12}	0.27
Longitudinal thermal expansion coefficient, α_1 ($10^{-6}/°C$)	5.0
Transverse thermal expansion coefficient, α_2 ($10^{-6}/°C$)	26.0
Longitudinal tensile strength, F_1^t (MPa)	1280
Transverse tensile strength, F_2^t (MPa)	49
Longitudinal compressive strength, F_1^c (MPa)	690
Transverse compressive strength, F_2^c (MPa)	158
In-plane shear strength, F_6 (MPa)	69
Ultimate longitudinal tensile strain, ϵ_1^t	0.029

Table 3
Phase properties of S-glass epoxy ply

Material	Modulus E (GPa)	Poisson's ratio ν	Thermal expansion coefficient α ($10^{-6}/°C$)
Epoxy	3.5	0.33	44.49
S-glass	92.0	0.225	2.844

This corresponds to application of the thermal change, maximum allowable tensile force and optimized fiber prestress release.

In the linear elasticity problems considered, the magnitudes of all local stresses are proportional to those of applied mechanical or thermal loads, hence the results can be easily scaled and superimposed to reflect effects of loading combinations that do not violate the ply strength limits (74)–(76). The objective is to keep stresses induced by $\Delta\theta = -150°C$ together with optimized fiber prestress distribution found in step (b), and stresses found in step (c), within the ply strength limits. Similar limits imposed on the interior stresses are best evaluated and visualized in terms of initial damage envelopes for the laminates, constructed below according to the procedure described by Dvorak and Suvorov (2000).

6.2. Free edge stresses due to cooling

Figs. 3 and 4 present the free edge stresses caused in the two laminates by $\Delta\theta = -150°C$ cooling from matrix curing temperature. Note that relatively large local shear stress concentration are indicated in the laminates. The fiber prestress applied to all plies that completely cancels all interlaminar stresses in the entire laminate is found from Eq. (11), using the ply properties listed in Table 2 and Appendix A, as $(\sigma_{11}^f)_P^i = 239.08$ MPa. Note that this value depends only on ply properties and is independent of ply orientation and laminate layup. This prestress is well below the fiber strength of at least 2800 MPa, implied by the fiber volume fraction and ply tensile strength listed in Table 2. While generally well within the strength limits listed in Table 2, some of the computed stresses are significant parts of the total stress under both thermal and mechanical loads. For example, the longitudinal shear σ_{xz} at the $(+45/-45)$ interface in Fig. 4 is equal to 32.36 MPa at the laminate free edge, or 47% of the shear strength F_6 in Table 2. Later, in Fig. 13, superposition of this stress with that induced by an applied tension force helps to reduce the high shear stresses contributed by a tension force applied in the X-direction.

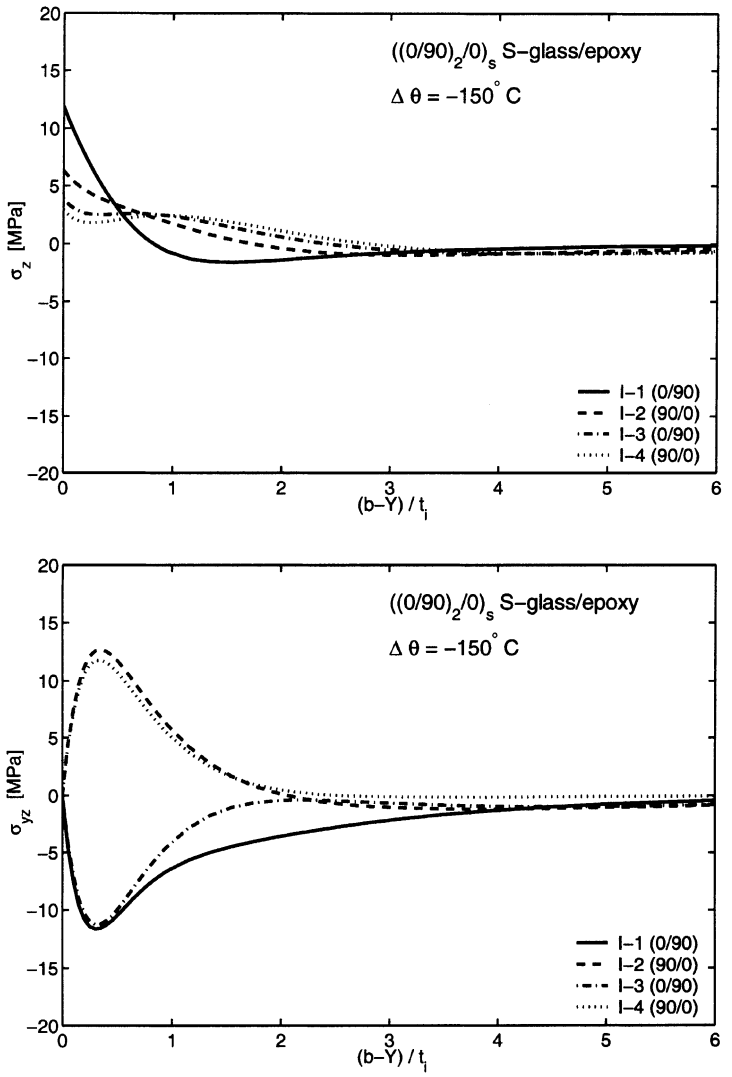

Fig. 3. Interlaminar stresses at the free edge $Y = \pm b$ of $((0/90)_2/\bar{0})_s$ S-glass/epoxy laminate cooled by $\Delta\theta = -150°C$ from fabrication to ambient temperature. These are reduced to zero by release of fiber prestress $(\sigma_{11}^f)_P^i = 239.08$ MPa applied to all plies.

6.3. Free edge stresses due to thermomechanical loads and release of optimized fiber prestress

In the examples that follow, the two laminates are loaded by both the above thermal change, a certain tensile stress N_x/t applied at the clamped edges $X = \pm a$, and an optimized fiber prestress. Both the mechanical load and the fiber prestress are sought such that the former is maximized or equal to zero, while release of the fiber prestress guarantees that the ply strength limits (74)–(76) are not violated either in the interior or at the free edges $Y = \pm b$ of the laminate.

The solution procedure is best illustrated by considering the $((0/90)_2/\bar{0})_s$ laminate. First, an initial damage envelope is constructed for this laminate, loaded only by the temperature change $\Delta\theta = -150°C$ and

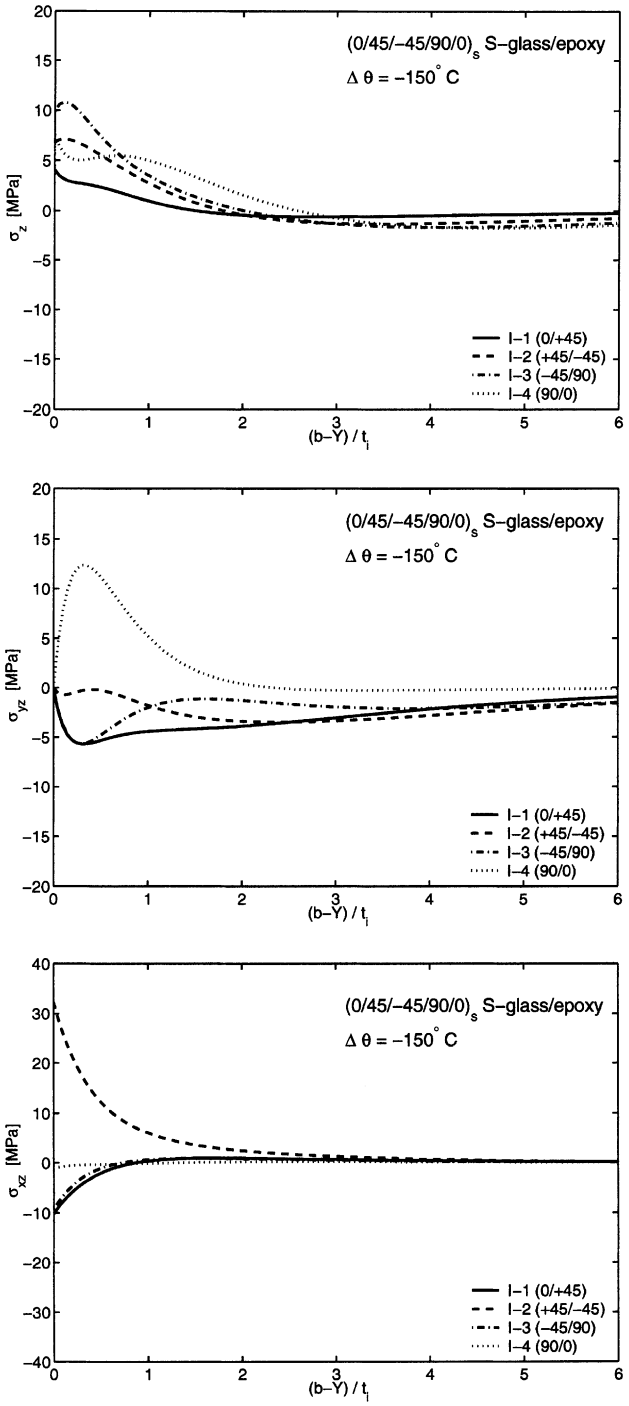

Fig. 4. Interlaminar stresses at the free edge $Y = \pm b$ of $(0/45/-45/90/\bar{0})_s$ S-glass/epoxy laminate cooled by $\Delta\theta = -150°C$ from fabrication to ambient temperature. These are reduced to zero by release of fiber prestress $(\sigma_{11}^f)_P^i = 239.08$ MPa applied to all plies.

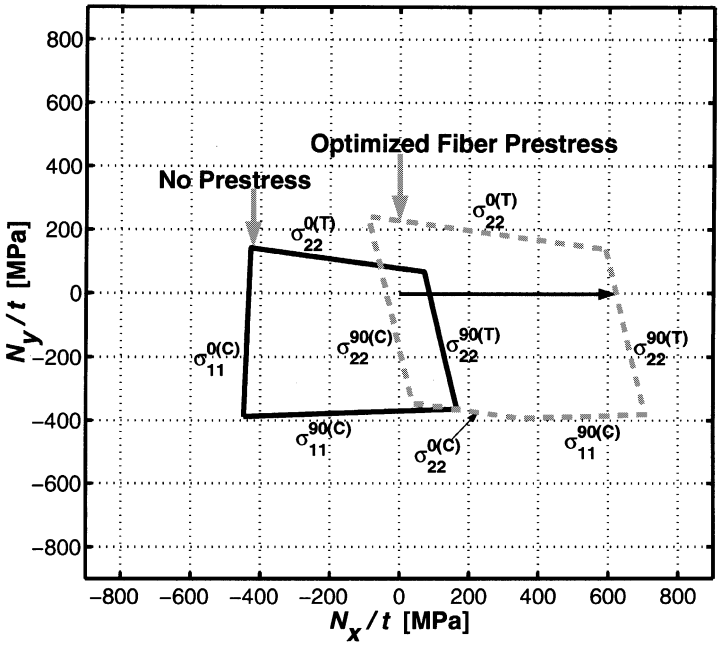

Fig. 5. Initial damage envelope for the $((0/90)_2/\bar{0})_s$ S-glass/epoxy laminate without prestress and after optimized prestress release. Optimized fiber prestress is equal to 2100 MPa in the 0° plies and to 357 MPa in the 90° plies. Thermal change of $\Delta\theta = -150$°C was applied in both cases.

by in-plane biaxial normal stresses N_x/t and N_y/t, without prestress, following the procedure in Dvorak and Suvorov (2000). This envelope in Fig. 5 consists of branches based on ply strength magnitudes listed in Table 2. For example, the $\sigma_{11}^{0(C)}$ branch indicates where the overall stresses cause local compressive stress in the 0° ply equal to the longitudinal compressive strength $F_1^c = 690$ MPa, Table 2. As expected the interior branches that form this envelope under biaxial overall tension correspond to the transverse tension strengths of the 0° and 90° plies. Under biaxial overall compression, the longitudinal compressive stress in both ply orientations far exceeds the transverse compressive stresses, hence the longitudinal compressive strength branches become the interior branches. A similar result was found in a $(\bar{0}/90)_{2s}$ laminate (*op. cit.*, Fig. 2), with the ply transverse strength branches entering the interior position near the left bottom corner of the envelope, under nearly isotropic biaxial compression.

This initial damage envelope indicates the approximate initial magnitude of the tension force N_x/t that can be safely applied to this laminate. Next, a sufficiently large prestress value is estimated and applied in the 0° plies together with $\Delta\theta = -150$°C and the corresponding prestress of 239.08 MPa in the 90° plies, such that after release of this prestress, the interior average ply stresses do not exceed the limits listed in Table 2. This condition is examined again with a new initial damage envelope. The estimated prestress in the 0° plies is then prescribed in the optimization procedure, and the optimal prestress values are found in the off-axis plies by solving the optimization problem (73)–(76). The initial damage envelope is then reconstructed for the laminate loaded by this optimized prestress; some strength branches may now assume new interior position which defines the strength envelope. The maximum value of N_x/t that can be safely applied may change, and if so, the optimization problem is solved with the updated value. The iteration is terminated when the loading vector is entirely within the damage envelope, so that the laminate remains damage free during mechanical loading.

Table 4
Optimized fiber prestress magnitudes, $(\sigma_{11}^f)_P^i$

$((0/90)_2/\bar{0})_s$ S-glass/epoxy at $N_x/t = 616.6$ MPa and $\Delta\theta = -150$°C (a)	$(0/45/-45/90/\bar{0})_s$ S-glass/epoxy at $N_x/t = 397.64$ MPa and $\Delta\theta = -150$°C (b)
0° plies: 2100 MPa 90° plies: 357 MPa	0° plies: 2000 MPa 90° plies: 540.8 MPa 45° plies: 272.2 MPa −45° plies: 275.9 MPa

For the $((0/90)_2/\bar{0})_s$ laminate, this iterative procedure has finally produced the initial damage envelope shown for the optimized fiber prestress in Fig. 5. All prestress values are stresses applied to fibers before and during matrix consolidation. Note that the branches now defining the compression strength are, in part, different from those in the laminate with no prestress. More significantly, the maximum tensile stress $N_x/t =$ 616.6 MPa can now be safely applied, together with the transverse stresses indicated by the initial damage envelope of the prestressed laminate. This far exceeds the value of 86.58 MPa that would be admitted without damage in the laminate without prestress. Table 4(a) indicates the maximum tension and the optimized ply prestresses. A relatively high magnitude of fiber prestress in the 0° plies is required to reduce the 90° ply stresses due to thermomechanical load. However, at $c_f = 0.4461$, and $F_1^t = 1280$ MPa, the implied fiber strength exceeds 2800 MPa, which is well above the levels indicated in Table 4(a).

Fig. 6 shows the optimized prestress values as function of the maximum applied normal strain in the 0° direction. In the present case, this was chosen as $\epsilon_x = 0.022$ or 0.75 of the ultimate strain for this laminate, and was reached under the $N_x/t = 616.6$ MPa.

Figs. 7 and 8 show the distributions of the interlaminar stresses σ_z and σ_{yz} at all ply interfaces, under (a) the maximum force and thermal change, assuming no damage, (b) after release of the optimized prestress and under thermal change alone, and (c) under the maximum tension force superimposed upon state (b). It

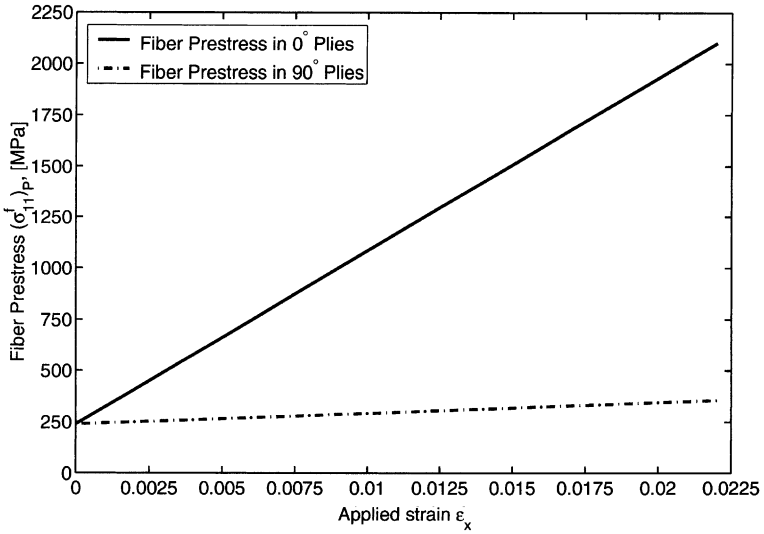

Fig. 6. Distribution of optimized fiber prestress in the plies of the $((0/90)_2/\bar{0})_s$ S-glass/epoxy laminate as function of the applied strain ϵ_x in the 0° direction.

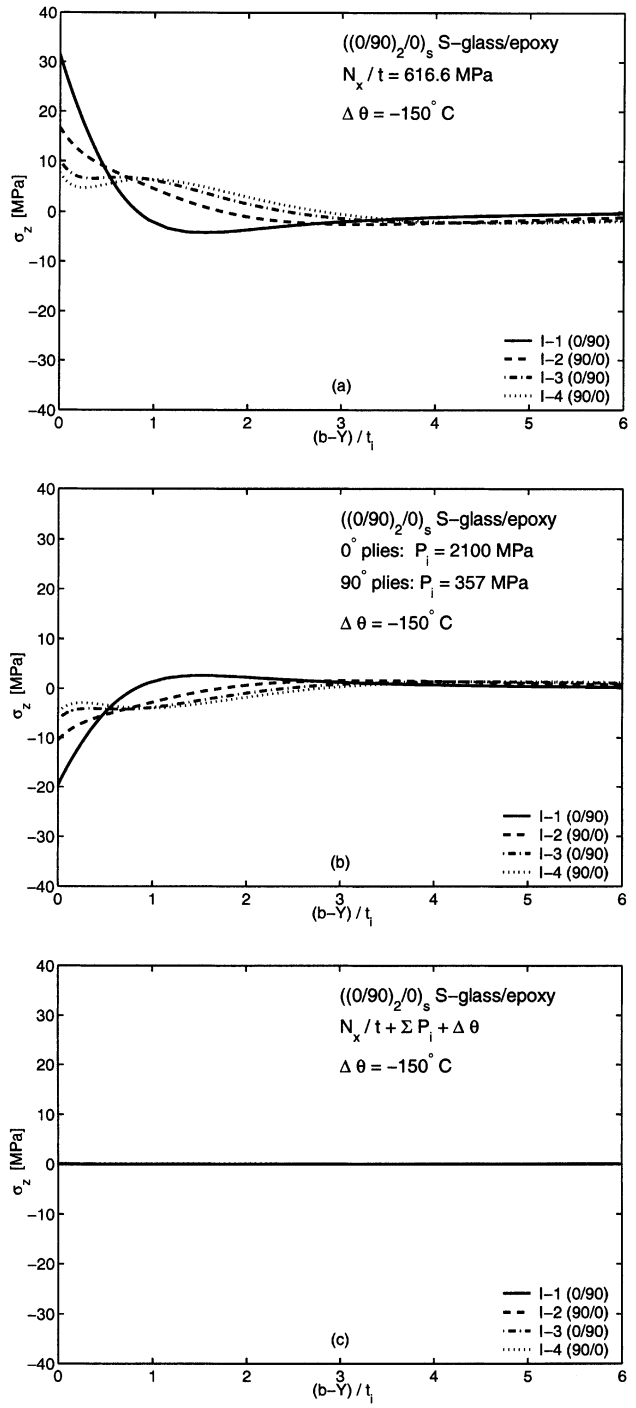

Fig. 7. Interlaminar stress σ_z at the free edge $Y = \pm b$ of the $((0/90)_2/\bar{0})_s$ S-glass/epoxy laminate caused by: (a) applied tensile force and temperature change; (b) release of fiber prestress and temperature change; (c) by tensile force, release of fiber prestress and temperature change. P_i is the fiber prestress magnitude.

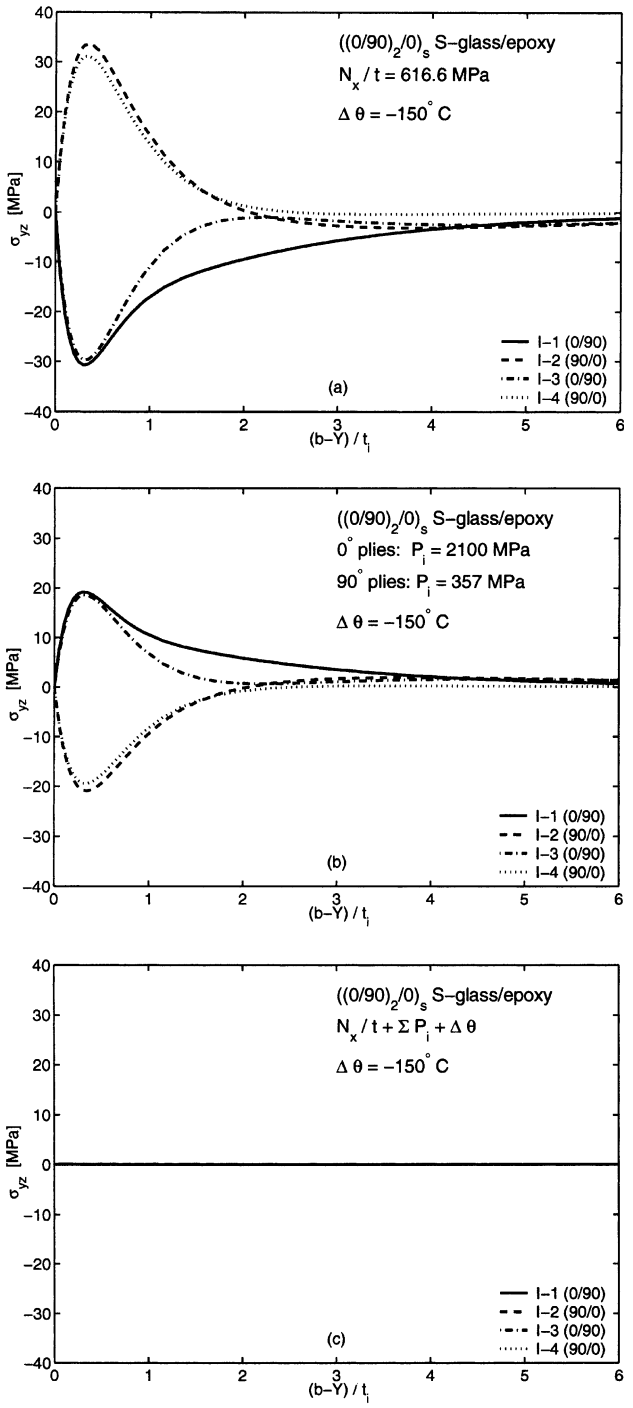

Fig. 8. Interlaminar stress σ_{yz} at the free edge $Y = \pm b$ of the $((0/90)_2/\bar{0})_s$ S-glass/epoxy laminate caused by: (a) applied tensile force and temperature change; (b) release of fiber prestress and temperature change; (c) by tensile force, release of fiber prestress and temperature change. P_i is the fiber prestress magnitude.

Table 5
Interlaminar stresses in the $((0/90)_2/\bar{0})_s$ laminate

	$[\sigma_z$ at $Y = b]$				$[\sigma_{yz}$ at $Y = b - t_i/3]$			
Interface	$\Delta\theta$	N_x	$P_i + \Delta\theta$	Σ	$\Delta\theta$	N_x	$P_i + \Delta\theta$	Σ
I-1	11.9	19.61	−19.61	0	−11.6	−19.11	19.11	0
I-2	6.34	10.44	−10.44	0	12.69	20.9	−20.9	0
I-3	3.85	6.35	−6.35	0	−11.23	−18.51	18.51	0
I-4	2.9	4.78	−4.78	0	11.8	19.44	−19.44	0

$\Delta\theta = -150°C$, $N_x/t = 616.6$ MPa, $\Sigma = N_x/t + P_i + \Delta\theta$, $P_i = (\sigma_{11}^f)_P^i$, 0° plies: 2100 MPa, 90° plies: 357 MPa.

Table 6
Average ply and fiber stresses in the $((0/90)_2/\bar{0})_s$ laminate

	$\Delta\theta$	N_x	$P_i + \Delta\theta$	Σ
0 ply: σ_1	−17.47	955.13	117.03	1072.2
0 ply: σ_{11}^f	−81.59	2031.22	319.67	2350.89
0 ply: σ_2	20.53	33.82	−33.82	0
90 ply: σ_1	−25.66	−42.27	42.27	0
90 ply: σ_{11}^f	−99.47	−146.18	110.91	−35.26
90 ply: σ_2	21.84	193.44	−146.29	47.15

$\Delta\theta = -150°C$, $N_x/t = 616.6$ MPa, $\Sigma = N_x/t + P_i + \Delta\theta$, $P_i = (\sigma_{11}^f)_P^i$, 0° plies: 2100 MPa, 90° plies: 357 MPa.

is evident that application of the maximum allowable mechanical load actually reduces the interlaminar free edge stresses in the prestressed laminate to zero. The optimized prestress and thermal change cause much smaller stresses than the mechanical and thermal loads in the absence of prestress.

Tables 5 and 6 show the numerical values of the interfacial stress maxima and average ply and fiber stresses caused by the individual loading components. The σ_{yz} maximum is typically located at the distance equal to 1/3 ply thickness from the free edge, or at $Y = b - t_i/3$. Note that under $N_x/t = 616.6$ MPa, the maximum tensile stress in the 0° ply increases from 955.13 (assuming no damage) to 1072.2 MPa, or by 12%, in the presence of the optimized fiber prestress. The latter value is lower than the ply tensile strength of 1280 MPa. Also shown in Table 6 are the fiber stress values contributed by the load components. The residual stresses retained after release of fiber prestress are much lower than the original prestress, and thus make only a small contribution to the total fiber stress during subsequent thermomechanical loading.

The prestressed laminate remains free of damage at the load level $N_x/t = 616.6$ MPa, which would have caused extensive internal damage and perhaps free edge delaminations in the absence of prestress. Of course, the 0° ply would carry a far higher part of the applied stress in a damaged laminate.

Figs. 9–13 and Tables 4(b), 7 and 8 present results for the $(0/45/-45/90/\bar{0})_s$ stacking sequence of the S-glass epoxy laminate. The procedure followed involved evaluation of the initial damage envelope after thermal change but with no prestress, an estimate of the maximum fiber prestress value in the 0° plies, finding of the optimized prestress values in the off-axis plies, replotting of the initial damage envelope for the prestressed laminate, and updating of the 0° fiber prestress. The initial and final positions of the damage envelopes are shown in Fig. 9. Again, different interior strength branches control compression strength, and as a result, the optimized prestress expands somewhat the "diameter" of the damage envelope in the direction of the N_x/t stress axis. In particular, application of fiber prestress in the 0° plies increases longitudinal tensile ply stresses in 0° plies compared to that caused by thermomechanical load applied without prestress (Table 8). This translates the compression branch $\sigma_{11}^{0(C)}$ in the direction opposite to that of the loading vector. In contrast, the prestress decreases transverse tensile stresses in the 90° plies. This translates

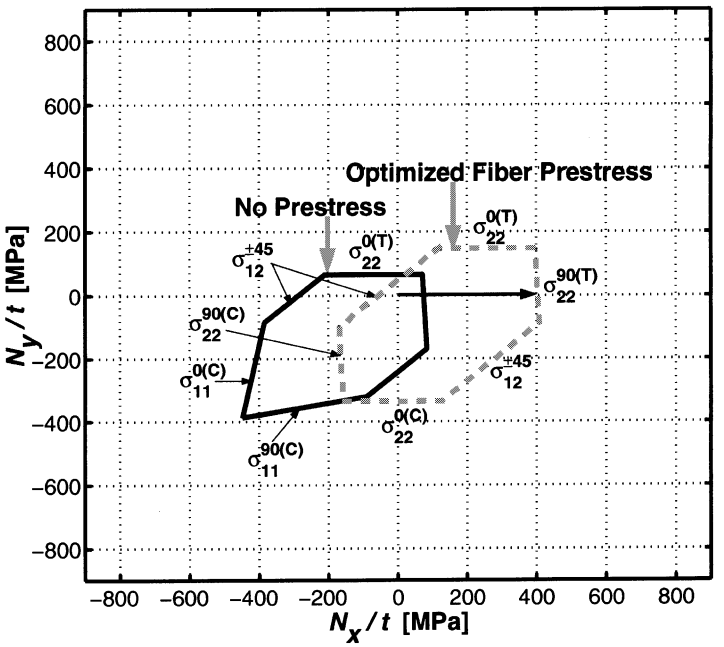

Fig. 9. Initial damage envelope for the $(0/45/-45/90/\bar{0})_s$ S-glass/epoxy laminate without prestress and after optimized prestress release. Optimized fiber prestress is equal to 2000 MPa in the 0° plies, 540.8 MPa in the 90° plies, 272.2 MPa in the 45° plies and 275.9 MPa in the −45° plies. Thermal change of $\Delta\theta = -150$°C was applied in both cases.

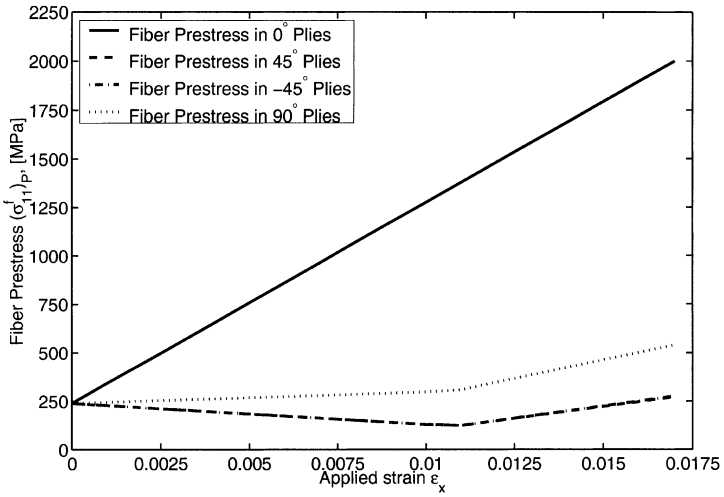

Fig. 10. Distribution of optimized fiber prestress in the plies of the $(0/45/-45/90/\bar{0})_s$ S-glass epoxy laminate as function of the applied strain ϵ_x in the 0° direction.

the compression branch $\sigma_{22}^{90(C)}$ in the direction of the loading vector. As a result, the $\sigma_{22}^{90(C)}$ strength branch controls in part the compressive strength of the prestressed laminate.

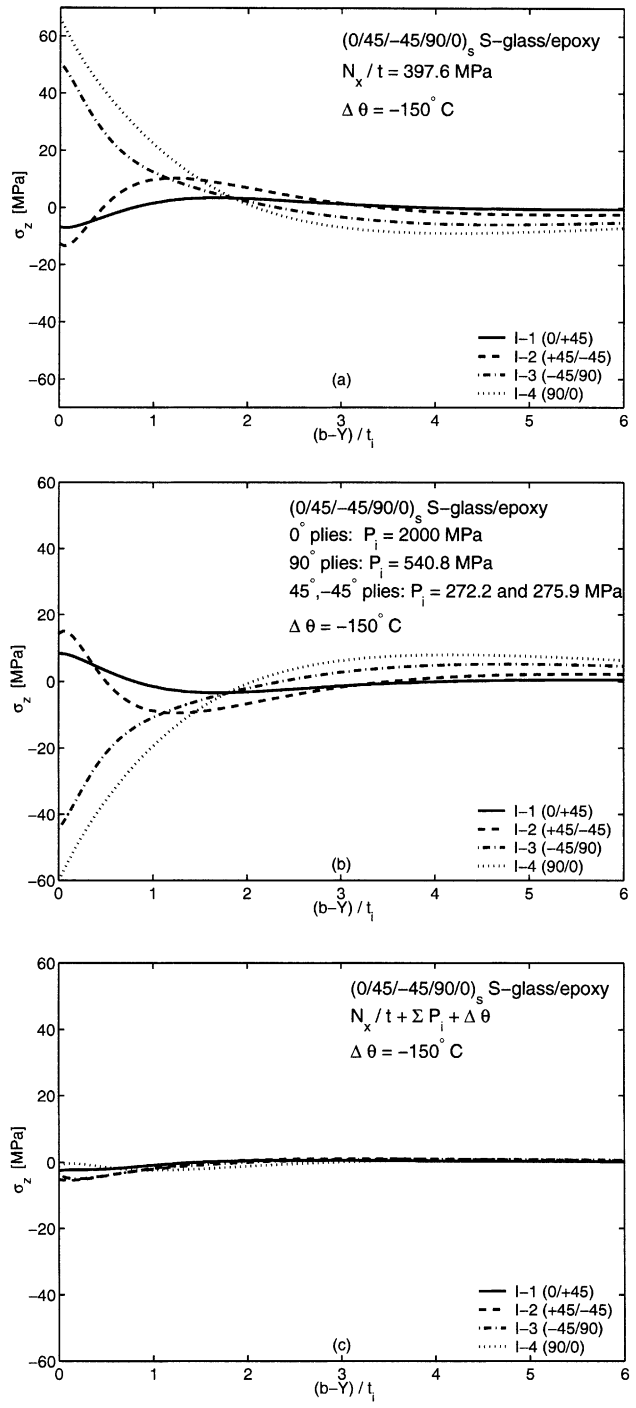

Fig. 11. Interlaminar normal stress σ_z at the free edge $Y = \pm b$ of the $(0/45/-45/90/\bar{0})_s$ laminate caused by: (a) applied tensile force N_x and temperature change; (b) release of fiber prestress and temperature change; (c) by tensile force, release of fiber prestress and temperature change. P_i is the fiber prestress magnitude.

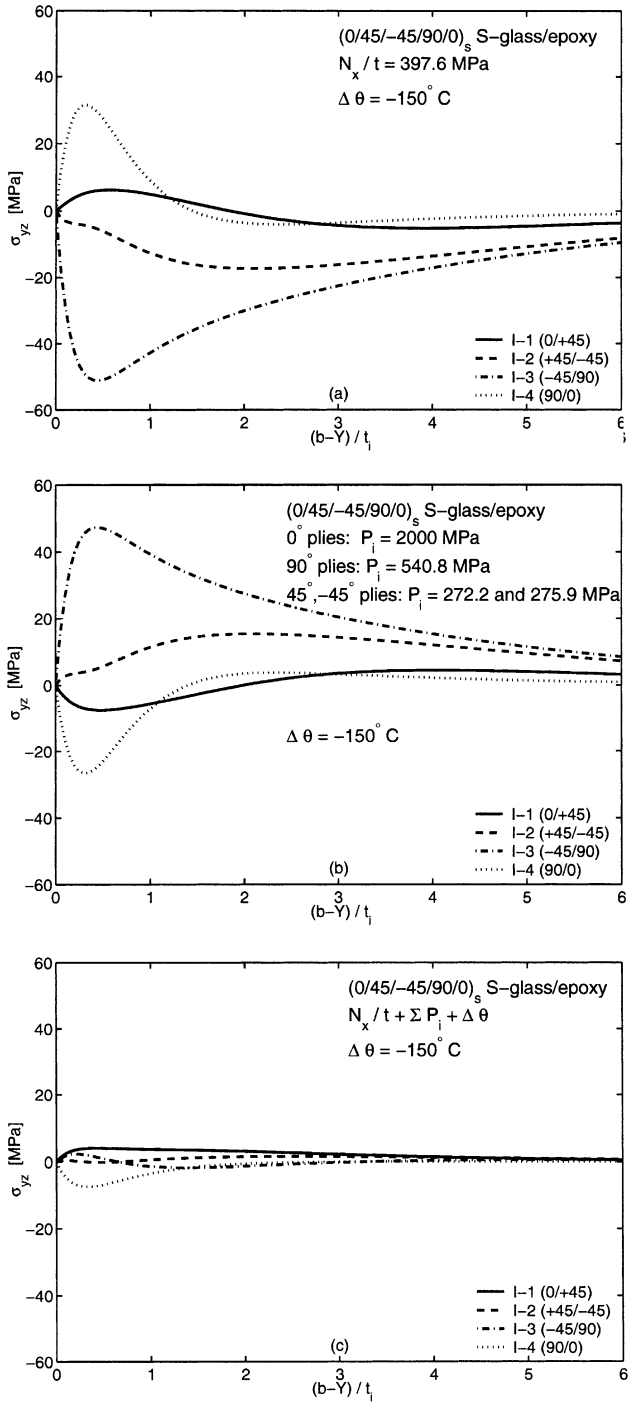

Fig. 12. Interlaminar shear stress σ_{yz} at the free edge $Y = \pm b$ of the $(0/45/-45/90/\bar{0})_s$ S-glass/epoxy laminate caused by: (a) applied tensile force N_x and temperature change; (b) release of fiber prestress and temperature change; (c) by tensile force, release of fiber prestress and temperature change. P_i is the fiber prestress magnitude.

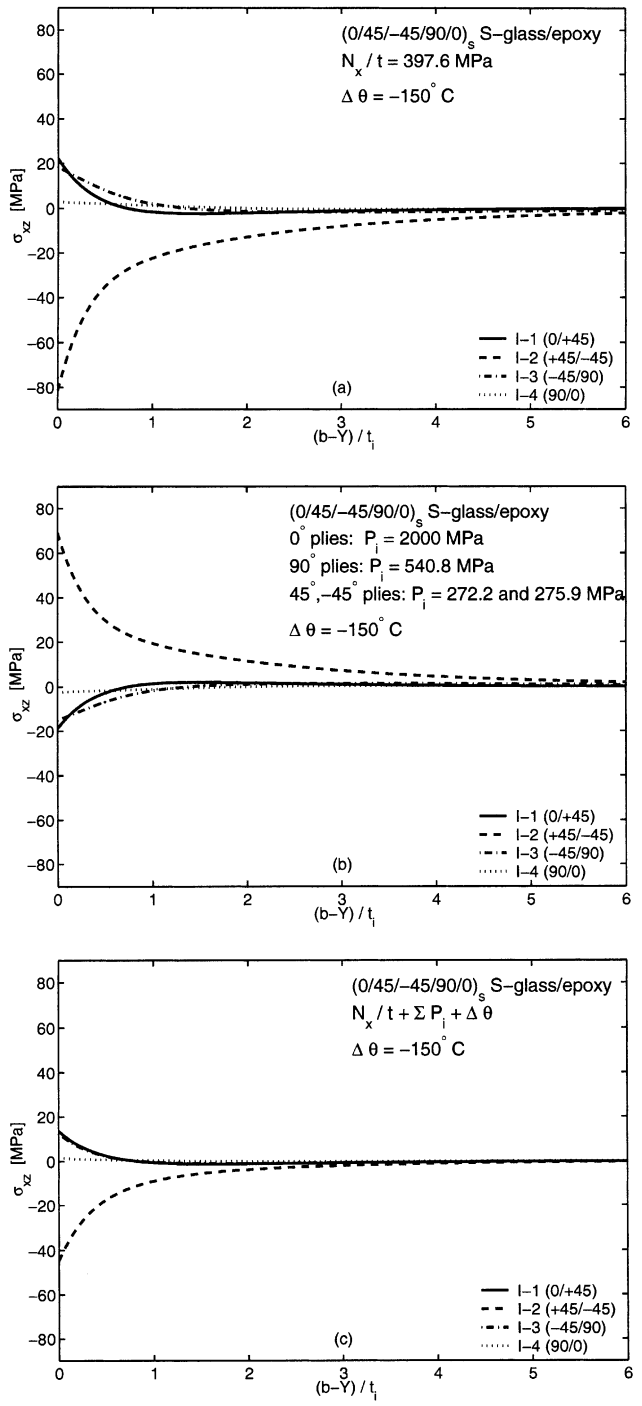

Fig. 13. Interlaminar shear stress σ_{xz} at the free edge $Y = \pm b$ of the $(0/45/-45/90/\bar{0})_s$ S-glass/epoxy laminate caused by: (a) applied tensile force N_x and temperature change; (b) release of fiber prestress and temperature change; (c) by tensile force, release of fiber prestress and temperature change. P_i is the fiber prestress magnitude.

Table 7
Interlaminar stresses in the $(0/45/-45/90/\bar{0})_s$ laminate

Interface	$[\sigma_z$ at $Y=b]$				$[\sigma_{yz}$ at $Y=b-t_i/3]$				$[\sigma_{xz}$ at $Y=b]$			
	$\Delta\theta$	N_x	$P_i+\Delta\theta$	Σ	$\Delta\theta$	N_x	$P_i+\Delta\theta$	Σ	$\Delta\theta$	N_x	$P_i+\Delta\theta$	Σ
I-1	4.05	−10.81	8.29	−2.52	−5.67	11.09	−7.11	3.98	−10.19	32.41	−18.78	13.63
I-2	6.79	−19.44	14.25	−5.18	−0.25	−4.2	4.19	−0.01	32.36	−113.68	69.0	−44.68
I-3	9.87	40.77	−44.37	−3.60	−5.61	−44.39	46.35	1.96	−9.27	27.56	−14.92	12.63
I-4	7.52	59.02	−60.04	−1.02	12.40	19.10	−26.59	−7.48	−1.15	4.08	−2.43	1.65

$\Delta\theta=-150$°C, $N_x/t=397.64$ MPa, $\Sigma=N_x/t+P_i+\Delta\theta$, $P_i=(\sigma_{11}^f)_P^i$, 0° plies: 2000 MPa, 90° plies: 540.8 MPa, +45° plies: 272.2 MPa, −45° plies: 275.9 MPa.

Table 8
Average ply and fiber stresses in the $(0/45/-45/90/\bar{0})_s$ laminate

	$\Delta\theta$	N_x	$P_i+\Delta\theta$	Σ
0 ply: σ_1	−16.0	730.90	310.73	1041.6
0 ply: σ_{11}^f	−78.39	1561.94	723.21	2285.14
0 ply: σ_2	20.24	−0.38	−14.04	−14.4
0 ply: σ_{12}	0.0	0.0	0.11	0.11
45 ply: σ_1	−21.68	285.07	−204.86	80.2
45 ply: σ_{11}^f	−90.78	588.66	−447.54	141.12
45 ply: σ_2	21.15	70.97	−54.88	16.09
45 ply: σ_{12}	−1.24	−97.35	55.61	−41.74
−45 ply: σ_1	−21.68	285.07	−204.18	80.88
−45 ply: σ_{11}^f	−90.78	588.66	−445.95	142.71
−45 ply: σ_2	21.15	70.97	−54.72	16.24
−45 ply: σ_{12}	1.24	97.35	−55.61	41.74
90 ply: σ_1	−27.36	−160.77	169.16	8.40
90 ply: σ_{11}^f	−103.17	−384.63	376.01	−8.61
90 ply: σ_2	22.06	142.31	−95.56	46.76
90 ply: σ_{12}	0.0	0.0	0.11	−0.11

$\Delta\theta=-150$°C, $N_x/t=397.64$ MPa, $\Sigma=N_x/t+P_i+\Delta\theta$, $P_i=(\sigma_{11}^f)_P^i$, 0° plies: 2000 MPa, 90° plies: 540.8 MPa, +45° plies: 272.2 MPa, −45° plies: 275.9 MPa.

Fig. 10 presents the optimized prestress distribution in the plies as a function of maximum applied strain, in the present case this was found as $\epsilon_x=0.017$, at the maximum allowable applied stress of $N_x/t=397.64$ MPa. This is lower than in the previous case, limited by the requirement that the loading vector remains within the damage envelope of the optimally prestressed laminate. The distribution of fiber prestress in Fig. 10 deviates significantly at $\epsilon_x>0.011$ from the linear or nearly linear character displayed in Fig. 6. This redistribution is enforced by the constraints (74)–(76) imposed by the ply strength criteria. While the lines for the +45 and −45 plies appear to coincide, they are actually somewhat different, as indicated in Figs. 11–13 and Table 4(b). This reflects the presence of different (0 and 90) ply orientations adjoining the 45 and −45 plies.

Figs. 11–13 show the distributions of interlaminar free edge stresses for (a) the maximum mechanical load and the thermal change, but no prestress, (b) optimized prestress, thermal change, but no mechanical load, and (c) prestress, mechanical load, and thermal change. The peel stress $\sigma_z=59.02+7.52=66.72$ MPa at the I-4 interface, under thermomechanical loads acting alone (Fig. 11a and Table 7) exceeds the ply transverse strength of 49 MPa. This is counteracted by the similarly high compressive normal stress generated at this interface by the optimized prestress in the presence of thermal change (Fig. 11b) so that nearly

zero normal stresses at all interfaces are found in the prestressed and mechanically loaded laminate, Fig. 11c. The shear stress $\sigma_{xz} = -113.68 + 32.36 = -81.32$ MPa at the interface I-2 in the loaded laminate without prestress (Fig. 13a and Table 7) is well above allowed value of $-F_6 = -69$ MPa in Table 2, but is reduced to this value by the optimized prestress.

The optimized fiber prestress distribution and interlaminar stresses were also found for 9-layer $(90/-45/0/45/\bar{0})_s$ S-glass epoxy laminate. The interlaminar stress magnitudes appearing in Figs. 12a and 13a and those found for the $(90/-45/0/45/\bar{0})_s$ system support the observation made by Herakovich (1989, 1998) that the laminate with adjacent $\pm 45°$ layers is particularly susceptible to large shear stress concentrations, more so than the system with interspersed $\pm 45°$ layers. Therefore, application of fiber prestress for interlaminar stress reduction appears to be most beneficial in the $(0/45/-45/90/\bar{0})_s$ layup.

It is worth mentioning that the fiber prestress can be useful in reduction of free edges stresses caused by compressive axial loading N_x/t. This is especially true for quasi-isotropic laminates. Prestress of $0°$ plies would have to be decreased whereas prestress of ± 45-plies increased. In fact, it was found that distribution of optimized fiber prestress plotted over the range of negative axial strain is a continuation of the lines shown in Figs. 6 and 10 for positive values of axial strain. However, since the prestress of $0°$ plies becomes small or zero the damage envelope will not be translated in any significant way towards larger magnitudes of the maximum allowable compressive stress N_x/t.

We note in passing that the procedure has also been applied to laminates made of high modulus carbon/epoxy plies. The damage envelopes found by optimizing the fiber prestress are often much larger than those for such laminates without prestress. Results will appear elsewhere.

7. Closure

Analysis of free edge stress concentrations was presented for laminates subjected to thermal changes, ply eigenstrains, release of fiber prestress that was applied prior to matrix consolidation in individual plies, and to mechanical loads. The thermal and transformation loads were converted into a superposition of certain uniform fields with solutions of related mechanical loading problems. Release of fiber prestress induces equivalent overall compression at the edges of each prestressed ply.

A procedure was described for evaluation of optimized fiber prestress distribution in individual plies of the laminate, which when released, creates residual stresses that suppress both damage development in the interior of the laminate and interlaminar delamination at the free edges. The free edge residual stresses remain within certain allowable limits while the laminate is unloaded, and actually decrease under applied mechanical loads. The interior residual stresses caused by prestress release are similar to those induced by equivalent overall in-plane compression. In superposition with applied overall tension, these stresses reduce and keep the ply stresses within allowable limits at overall loads far exceeding those allowed in laminates without prestress. Although the examples shown were constructed for loading by a uniaxial tension, the resulting damage envelopes can be utilized in applications involving cyclic loading programs that involve additional overall loads, as long as the loading path is altogether bounded by the damage envelope. Of course, the method can also be employed in finding maximum load amplitudes for programs of cyclic loading dominated by a combination of overall stress components. The results clearly demonstrate the potential of fiber prestress in damage control and prevention in composite laminates. In conjunction with our earlier paper (Dvorak and Suvorov, 2000), they provide a concise methodology for design of optimal prestress distribution that can substantially improve resistance to both interior damage and free edge delaminations in laminated plates. They also suggest need for prevention of undesirable and potentially harmful residual stresses, by careful analysis and control of laminate fabrication processes.

Acknowledgements

This work was supported by the Army Research Office under agreement no. DAAG 55-98-0464. Dr. Mohammed Zikry served as program monitor.

Appendix A

Denote the local coordinate system of the transversely isotropic unidirectional composite material by (x_1, x_2, x_3). Suppose the fiber axis coincides with x_1 axis of the system. Then the compliance matrix of the transversely isotropic ply written in the local coordinate system is defined as follows,

$$\begin{pmatrix} \epsilon_{11} \\ \epsilon_{22} \\ \epsilon_{33} \\ 2\epsilon_{23} \\ 2\epsilon_{13} \\ 2\epsilon_{12} \end{pmatrix} = \begin{pmatrix} 1/E_1 & -v_{12}/E_1 & -v_{12}/E_1 & 0 & 0 & 0 \\ -v_{12}/E_1 & 1/E_2 & -v_{23}/E_2 & 0 & 0 & 0 \\ -v_{12}/E_1 & -v_{23}/E_2 & 1/E_2 & 0 & 0 & 0 \\ 0 & 0 & 0 & 1/G_{23} & 0 & 0 \\ 0 & 0 & 0 & 0 & 1/G_{12} & 0 \\ 0 & 0 & 0 & 0 & 0 & 1/G_{12} \end{pmatrix} \begin{pmatrix} \sigma_{11} \\ \sigma_{22} \\ \sigma_{33} \\ \sigma_{23} \\ \sigma_{13} \\ \sigma_{12} \end{pmatrix} \tag{A.1}$$

Engineering constants E_1, v_{12}, E_2 and G_{12} are given in Table 2 for S-glass epoxy ply. Compliance matrix given by Eq. (A.1) transforms into the overall coordinate system according to the third term in Eq. (2). The transformation matrices are defined as,

$$\boldsymbol{T} = \begin{pmatrix} c^2 & s^2 & 0 & 0 & 0 & 2cs \\ s^2 & c^2 & 0 & 0 & 0 & -2cs \\ 0 & 0 & 1 & 0 & 0 & 0 \\ 0 & 0 & 0 & c & -s & 0 \\ 0 & 0 & 0 & s & c & 0 \\ -cs & cs & 0 & 0 & 0 & c^2 - s^2 \end{pmatrix} \quad \boldsymbol{R} = [\boldsymbol{T}^{-1}]^{\mathrm{T}}$$
$$c = \cos(\phi), \qquad s = \sin(\phi) \tag{A.2}$$

and the angle ϕ is measured from the laminate 0° direction X to the x_1 fiber direction in the ply.

Hill's (1964) elastic moduli of the transversely isotropic plies are defined as

$$k = -[1/G_{23} - 4/E_2 + 4v_{12}^2/E_1]^{-1} \quad l = 2kv_{12} \quad n = E_1 + l^2/k \quad m = G_{23} \quad p = G_{12}$$

The elastic moduli of matrix or fiber phases will be denoted by the same letters but with the subscripts m of f, respectively.

We assume that the S-glass fiber and epoxy matrix are isotropic phases constituting the ply with the properties given in Table 3.

Evidently, the fifth constant – the transverse Poisson's ratio v_{23} is required to completely define compliance matrix in Eq. (A.1). The effective stiffness of the composite ply and the missing transverse Poisson's ratio v_{23} are found by one of the averaging methods described in Dvorak and Srinivas (1999). These methods regard each phase as an inclusion residing in a large volume of comparison medium with selected elastic moduli and the comparison medium itself is an inclusion embedded in a very large volume of the effective medium. The elastic properties of the effective medium are identified with those of the composite ply given in Table 2. The following choice of elastic moduli of the comparison medium respects already existing elastic moduli of the composite ply (Table 2) and phase properties (Table 3): $p_0 = 3.6084$, $m_0 = 2.8005$, and $k_0 = 3.9621$, $n_0 = c_m n_m + c_f n_f = 50.0783$, $l_0 = l_m = 2.5542$ GPa. Also, fiber volume fraction c_f is set equal to $c_f = 0.4461$.

The elastic moduli of the composite ply can be found now,

$$
\begin{aligned}
p &= \frac{2c_f p_f(p_0+p_m)+2c_m p_m(p_0+p_f)}{2(c_m(p_0+p_f)+c_f(p_0+p_m))}\\
m &= \frac{m_0k_0(c_f m_f+c_m k_m)+m_f m_m(k_0+2m_0)}{m_0k_0+(k_0+2m_0)(c_f m_m+c_m m_f)}\\
k &= \frac{c_f k_f(k_m+m_0)+c_m k_m(k_f+m_0)}{c_f(m_0+k_m)+c_m(m_0+k_f)}\\
l &= \frac{c_f l_f(k_m+m_0)+c_m l_m(k_f+m_0)}{c_f(m_0+k_m)+c_m(m_0+k_f)}\\
n &= c_f n_f+c_m n_m+c_f l_f\left\{\frac{c_m(l_m-l_f)}{c_f(m_0+k_m)+c_m(m_0+k_f)}\right\}+c_m l_m\left\{\frac{c_f(l_f-l_m)}{c_f(m_0+k_m)+c_m(m_0+k_f)}\right\}
\end{aligned}
\tag{A.3}
$$

The ply stiffness matrix in the local coordinates then becomes,

$$
\boldsymbol{L}=\begin{pmatrix}
45.4481 & 4.5335 & 4.5335 & 0 & 0 & 0\\
4.5335 & 11.4862 & 5.3047 & 0 & 0 & 0\\
4.5335 & 5.3047 & 11.4862 & 0 & 0 & 0\\
0 & 0 & 0 & 3.0908 & 0 & 0\\
0 & 0 & 0 & 0 & 4.5 & 0\\
0 & 0 & 0 & 0 & 0 & 4.5
\end{pmatrix}
\tag{A.4}
$$

and the compliance matrix,

$$
\boldsymbol{S}=\begin{pmatrix}
0.0233 & -0.0063 & -0.0063 & 0 & 0 & 0\\
-0.0063 & 0.1124 & -0.0494 & 0 & 0 & 0\\
-0.0063 & -0.0494 & 0.1124 & 0 & 0 & 0\\
0 & 0 & 0 & 0.3235 & 0 & 0\\
0 & 0 & 0 & 0 & 0.2222 & 0\\
0 & 0 & 0 & 0 & 0 & 0.2222
\end{pmatrix}
\tag{A.5}
$$

Transverse Poisson's ratio immediately follows as,

$$
v_{23}=\frac{E_2}{2G_{23}}-1,\quad v_{23}=0.4398
\tag{A.6}
$$

The thermal expansion coefficients of the phases (Table 3) are found from experimentally measured expansion coefficients of the composite ply (Table 2) and the elastic moduli of the comparison medium by using formula derived by Levin (1967).

Appendix B

In this appendix we formulate restrictions on magnitude of force resultants N_{xy} at the edges $X=\pm a$ and N_{yx} at $Y=\pm b$ for the choice of stress field dependent on two variables Y and Z and derivable from two stress functions $F(Y,Z)$ and $\Psi(Y,Z)$ as indicated by Eq. (28). As before, we analyze the stress field on the plane $X=0$ bounded by two parallel edges $Y=\pm b$ and top and bottom surfaces of the plate.

We start with the force resultant N_{yx}. If shear stresses σ_{yx}^{si} are applied at the edges $Y = \pm b$, then for arbitrary value of Y coordinate,

$$N_{yx} = \int_{z_0}^{z_N} \sigma_{yx}^{si}\,\mathrm{d}Z = \int_{z_0}^{z_N} \sigma_{yx}\,\mathrm{d}Z = \sum_{i=1}^{N} \int_{z_{i-1}}^{z_i} \sigma_{yx}^{i}\,\mathrm{d}Z = \sum_{i=1}^{N} \int_{z_{i-1}}^{z_i} \Psi_{,z}^{i}\,\mathrm{d}Z = \Psi_N - \Psi_0 \tag{B.1}$$

On the other hand,

$$\begin{aligned} N_{xy} &= \int_{z_0}^{z_N} \sigma_{xy}^{si}\,\mathrm{d}Z + N_{xy}^{m} = \int_{z_0}^{z_N} \int_{Y=-b}^{Y=b} \sigma_{xy}\,\mathrm{d}Y\,\mathrm{d}Z = \sum_{i=1}^{N} \int_{z_{i-1}}^{z_i} \int_{Y=-b}^{Y=b} \sigma_{xy}^{i}\,\mathrm{d}Y\,\mathrm{d}Z \\ &= \sum_{i=1}^{N} \int_{z_{i-1}}^{z_i} \int_{Y=-b}^{Y=b} \Psi_{,z}^{i}\,\mathrm{d}Y\,\mathrm{d}Z = \sum_{i=1}^{N} \int_{\gamma_i} \Psi^{i} \cos(n, Z)\,\mathrm{d}s = \Psi_N - \Psi_0 \end{aligned} \tag{B.2}$$

where γ_i is the contour of ith ply on the plane $X = 0$. From Eqs. (B.1) and (B.2) it follows that the loading conditions should be such that,

$$N_{yx} = \int_{z_0}^{z_N} \sigma_{yx}^{si}\,\mathrm{d}Z = N_{xy} = \int_{z_0}^{z_N} \sigma_{xy}^{si}\,\mathrm{d}Z + N_{xy}^{m} \tag{B.3}$$

It is seen that if the stress field is derivable from two stress functions $F(Y, Z)$ and $\Psi(Y, Z)$, as indicated by Eq. (28), then the shear force resultant N_{xy} must be equal to N_{yx}.

For prestressed laminated plate subjected to ply transformation fields,

$$\int_{z_0}^{z_N} \sigma_{yx}^{si}\,\mathrm{d}Z = \int_{z_0}^{z_N} \sigma_{xy}^{si}\,\mathrm{d}Z \tag{B.4}$$

and, hence,

$$N_{xy}^{m} = 0 \tag{B.5}$$

Thus, actually applied shearing force resultant at the edges $X = \pm a$ must be zero provided that no mechanical loads are applied at the edges $Y = \pm b$.

Appendix C

We write the matrices in the system of differential equations (51) in the blockwise manner,

$$\begin{aligned} &\begin{bmatrix} \boldsymbol{w}^{FF} & \boldsymbol{w}^{FG} & 0 & 0 \\ \boldsymbol{w}^{GF} & \boldsymbol{w}^{GG} & 0 & 0 \\ 0 & 0 & 0 & 0 \\ 0 & 0 & 0 & 0 \end{bmatrix} \begin{bmatrix} \boldsymbol{F}^{IV} \\ \boldsymbol{G}^{IV} \\ \boldsymbol{\Psi}^{IV} \\ \boldsymbol{H}^{IV} \end{bmatrix} + \begin{bmatrix} \boldsymbol{v}^{FF} & \boldsymbol{v}^{FG} & \boldsymbol{v}^{F\Psi} & \boldsymbol{v}^{FH} \\ \boldsymbol{v}^{GF} & \boldsymbol{v}^{GG} & \boldsymbol{v}^{G\Psi} & \boldsymbol{v}^{GH} \\ \boldsymbol{v}^{\Psi F} & \boldsymbol{v}^{\Psi G} & \boldsymbol{v}^{\Psi\Psi} & \boldsymbol{v}^{\Psi H} \\ \boldsymbol{v}^{HF} & \boldsymbol{v}^{HG} & \boldsymbol{v}^{H\Psi} & \boldsymbol{v}^{HH} \end{bmatrix} \begin{bmatrix} \boldsymbol{F}^{II} \\ \boldsymbol{G}^{II} \\ \boldsymbol{\Psi}^{II} \\ \boldsymbol{H}^{II} \end{bmatrix} \\ &+ \begin{bmatrix} \boldsymbol{u}^{FF} & \boldsymbol{u}^{FG} & \boldsymbol{u}^{F\Psi} & \boldsymbol{u}^{FH} \\ \boldsymbol{u}^{GF} & \boldsymbol{u}^{GG} & \boldsymbol{u}^{G\Psi} & \boldsymbol{u}^{GH} \\ \boldsymbol{u}^{\Psi F} & \boldsymbol{u}^{\Psi G} & \boldsymbol{u}^{\Psi\Psi} & \boldsymbol{u}^{\Psi H} \\ \boldsymbol{u}^{HF} & \boldsymbol{u}^{HG} & \boldsymbol{u}^{H\Psi} & \boldsymbol{u}^{HH} \end{bmatrix} \begin{bmatrix} \boldsymbol{F} \\ \boldsymbol{G} \\ \boldsymbol{\Psi} \\ \boldsymbol{H} \end{bmatrix} = \boldsymbol{b} \end{aligned} \tag{C.1}$$

Substitution of Eq. (55) into homogeneous part of Eq. (C.1) leads to the system of algebraic equations,

$$\omega^4\begin{bmatrix} \boldsymbol{w}^{FF} & \boldsymbol{w}^{FG} & 0 & 0 \\ \boldsymbol{w}^{GF} & \boldsymbol{w}^{GG} & 0 & 0 \\ 0 & 0 & 0 & 0 \\ 0 & 0 & 0 & 0 \end{bmatrix}\begin{bmatrix} \boldsymbol{p}^F \\ \boldsymbol{p}^G \\ \boldsymbol{p}^\Psi \\ \boldsymbol{p}^H \end{bmatrix} + \omega^2\begin{bmatrix} \boldsymbol{v}^{FF} & \boldsymbol{v}^{FG} & \boldsymbol{v}^{F\Psi} & \boldsymbol{v}^{FH} \\ \boldsymbol{v}^{GF} & \boldsymbol{v}^{GG} & \boldsymbol{v}^{G\Psi} & \boldsymbol{v}^{GH} \\ \boldsymbol{v}^{\Psi F} & \boldsymbol{v}^{\Psi G} & \boldsymbol{v}^{\Psi\Psi} & \boldsymbol{v}^{\Psi H} \\ \boldsymbol{v}^{HF} & \boldsymbol{v}^{HG} & \boldsymbol{v}^{H\Psi} & \boldsymbol{v}^{HH} \end{bmatrix}\begin{bmatrix} \boldsymbol{p}^F \\ \boldsymbol{p}^G \\ \boldsymbol{p}^\Psi \\ \boldsymbol{p}^H \end{bmatrix}$$
$$+ \begin{bmatrix} \boldsymbol{u}^{FF} & \boldsymbol{u}^{FG} & \boldsymbol{u}^{F\Psi} & \boldsymbol{u}^{FH} \\ \boldsymbol{u}^{GF} & \boldsymbol{u}^{GG} & \boldsymbol{u}^{G\Psi} & \boldsymbol{u}^{GH} \\ \boldsymbol{u}^{\Psi F} & \boldsymbol{u}^{\Psi G} & \boldsymbol{u}^{\Psi\Psi} & \boldsymbol{u}^{\Psi H} \\ \boldsymbol{u}^{HF} & \boldsymbol{u}^{HG} & \boldsymbol{u}^{H\Psi} & \boldsymbol{u}^{HH} \end{bmatrix}\begin{bmatrix} \boldsymbol{p}^F \\ \boldsymbol{p}^G \\ \boldsymbol{p}^\Psi \\ \boldsymbol{p}^H \end{bmatrix} = \boldsymbol{0} \tag{C.2}$$

Denote $\rho = \omega^2$ and $\boldsymbol{q}^F = \rho\boldsymbol{p}^F$, $\boldsymbol{q}^G = \rho\boldsymbol{p}^G$. Then Eq. (C.2) can be reduced to the following,

$$\rho\begin{bmatrix} \boldsymbol{w}^{FF} & \boldsymbol{w}^{FG} & \boldsymbol{v}^{FF} & \boldsymbol{v}^{FG} & \boldsymbol{v}^{F\Psi} & \boldsymbol{v}^{FH} \\ \boldsymbol{w}^{GF} & \boldsymbol{w}^{GG} & \boldsymbol{v}^{GF} & \boldsymbol{v}^{GG} & \boldsymbol{v}^{G\Psi} & \boldsymbol{v}^{GH} \\ 0 & 0 & \boldsymbol{v}^{\Psi F} & \boldsymbol{v}^{\Psi G} & \boldsymbol{v}^{\Psi\Psi} & \boldsymbol{v}^{\Psi H} \\ 0 & 0 & \boldsymbol{v}^{HF} & \boldsymbol{v}^{HG} & \boldsymbol{v}^{H\Psi} & \boldsymbol{v}^{HH} \\ 0 & 0 & -\boldsymbol{I} & 0 & 0 & 0 \\ 0 & 0 & 0 & -\boldsymbol{I} & 0 & 0 \end{bmatrix}\begin{bmatrix} \boldsymbol{q}^F \\ \boldsymbol{q}^G \\ \boldsymbol{p}^F \\ \boldsymbol{p}^G \\ \boldsymbol{p}^\Psi \\ \boldsymbol{p}^H \end{bmatrix}$$
$$+ \begin{bmatrix} 0 & 0 & \boldsymbol{u}^{FF} & \boldsymbol{u}^{FG} & \boldsymbol{u}^{F\Psi} & \boldsymbol{u}^{FH} \\ 0 & 0 & \boldsymbol{u}^{GF} & \boldsymbol{u}^{GG} & \boldsymbol{u}^{G\Psi} & \boldsymbol{u}^{GH} \\ 0 & 0 & \boldsymbol{u}^{\Psi F} & \boldsymbol{u}^{\Psi G} & \boldsymbol{u}^{\Psi\Psi} & \boldsymbol{u}^{\Psi H} \\ 0 & 0 & \boldsymbol{u}^{HF} & \boldsymbol{u}^{HG} & \boldsymbol{u}^{H\Psi} & \boldsymbol{u}^{HH} \\ \boldsymbol{I} & 0 & 0 & 0 & 0 & 0 \\ 0 & \boldsymbol{I} & 0 & 0 & 0 & 0 \end{bmatrix}\begin{bmatrix} \boldsymbol{q}^F \\ \boldsymbol{q}^G \\ \boldsymbol{p}^F \\ \boldsymbol{p}^G \\ \boldsymbol{p}^\Psi \\ \boldsymbol{p}^H \end{bmatrix} = \boldsymbol{0} \tag{C.3}$$

Denoting the first matrix in Eq. (C.3) by $\boldsymbol{B}$ and second matrix by $\boldsymbol{A}$, Eq. (C.3) can be reduced to standard generalized eigenvalue problem,

$$\boldsymbol{A}\boldsymbol{x} = -\rho\boldsymbol{B}\boldsymbol{x} \tag{C.4}$$

where $\boldsymbol{x}$ is a $6n+1$ vector,

$$\boldsymbol{x} = \begin{bmatrix} \boldsymbol{q}^F \\ \boldsymbol{q}^G \\ \boldsymbol{p}^F \\ \boldsymbol{p}^G \\ \boldsymbol{p}^\Psi \\ \boldsymbol{p}^H \end{bmatrix} \tag{C.5}$$

Solution of the eigenvalue problem Eq. (C.4) yields $6n+1$ eigenvalues ρ and $6n+1$ eigenvectors $\boldsymbol{x}$. $6n+1$ eigenvalues ρ will produce $12n+2$ eigenvalues ω since $\rho = \omega^2$.

References

Alberski, T.C., 2000. Ph.D. Dissertation, Rensselaer Polytechnic Institute.

Brewer, J.C., Lagace, P.A., 1988. Quadratic stress criterion for initiation of delamination. J. Comp. Mater. 22, 1141–1155.

Cho, M., Kim, H.S., 2000. Iterative free-edge stress analysis of composite laminates under extension, bending, twisting and thermal loadings. Int. J. Solids Struct. 37, 435–459.

Christensen, R.M., 1979. Mechanics of Composite Materials. Wiley, New York.

Christensen, R.M., DeTeresa, S.J., 1992. Elimination/minimization of edge-induced stress singularities in fiber composite laminates. Int. J. Solids Struct. 29, 1221–1231.

Dvorak, G.J., Prochazka, P., Srinivas, M.V., 1999. Design and fabrication of submerged cylindrical laminates I. Int. J. Solids Struct. 36, 3917–3943.

Dvorak, G.J., Srinivas, M.V., 1999. New estimates of overall properties of heterogeneous solids. J. Mech. Phys. Solids 47, 899–920.

Dvorak, G.J., Suvorov, A.P., 2000. Effect of fiber prestress on residual stresses and onset of damage in symmetric laminates. Comp. Sci. Technol. 60 (8), 1129–1139.

Flanagan, G., 1994. An efficient stress function approximation for the free-edge stresses in laminates. Int. J. Solids Struct. 31, 941–952.

Gill, P.E., Murray, W., Wright, M.H., 1991. Numerical Linear Algebra and Optimization, vol. 1. Addison-Wesley, Redwood city, Calif.

Hayashi, T., 1967. Analytical study of interlaminar shear stresses in a laminate composite plate. Trans. Jpn. Soc. Aeronaut. Space Sci. 10 (17), 43–48.

Herakovich, C.T., 1989. Edge effects and delamination failures. J. Strain Anal. Engng. Des. 24 (4), 245–252.

Herakovich, C.T., 1998. Mechanics of Fibrous Composites. Wiley, New York, pp. 247–301.

Hill, R., 1964. Theory of mechanical properties of fibre-strengthened materials: I Elastic behavior. J. Mech. Phys. Solids 12, 199–212.

Kassapoglou, C., Lagace, P.A., 1986. An efficient method for the calculation of interlaminar stresses in composite materials. J. Appl. Mech. 53, 744–750.

Kim, T., Atluri, S.N., 1995a. Analysis of edge stresses in composite laminates under combined thermo-mechanical loading, using a complementary energy approach. Comput. Mech. 16, 83–97.

Kim, T., Atluri, S.N., 1995b. Optimal through-thickness temperature gradients for control of interlaminar stresses in composites. AIAA J. 33, 730–738.

Lekhnitskii, S.G., 1963. Theory of Elasticity of an Anisotropic Elastic Body (Trans. by P. Fern). Holden-Day, San Francisco.

Levin, V.M., 1967. Thermal expansion coefficients of heterogeneous materials. Izv. AN SSSR, Mekhanika Tverdogo Tela 2, 88–94. (English Translation) Mech. Solids 11, 58–61.

Noor, A.K., Burton, W.S., 1989. Assessment of shear deformation theories for multilayer composite plates. Appl. Mech. Rev. 42 (1), 1–13.

Pagano, N.J., 1978a. Stress fields in composite laminates. Int. J. Solids Struct. 14, 385–400.

Pagano, N.J., 1978b. Free edge stress fields in composite laminates. Int. J. Solids Struct. 14, 401–406.

Pipes, R.B., Pagano, N.J., 1970. Interlaminar stresses in composite laminates under uniform axial extension. J. Comp. Mater. 4, 538–548.

Reddy, J.N., 1997. Mechanics of Laminated Composite Plates: Theory and Analysis. CRC Press, New York.

Reissner, E., 1950. On variational theorem in elasticity. J. Mathe. Phys. 29, 90–95.

Rose, C.A., Herakovich, C.T., 1993. An approximate solution for interlaminar stresses in composite laminates. Comp. Engng. 3, 271–285.

Srinivas, M.V., Dvorak, G.J., Prochazka, P., 1999. Design and fabrication of submerged cylindrical laminates II. Effect of fiber prestress. Int. J. Solids Struct. 36, 3945–3976.

Vel, S.S., Batra, R.C., 2000. The generalized plane strain deformations of thick anisotropic composite laminated plates. Int. J. Solids Struct. 37, 715–733.

Wang, S.S., Choi, I., 1982. Boundary-layer effects in composite laminates: Part I. Free-edge stress singularities. J. Appl. Mech. 49, 541–548.

Wang, Y., Tarn, J., Hsu, C., 2000. State space approach for stress decay in laminates. Int. J. Solids Struct. 37, 3535–3553.

Whitney, J.M., 1988. Structural analysis of laminated composites. Technomic Publishing Company, Lancaster, Pa., US.

Ye, L., 1990. Some characteristics of distributions of free-edge interlaminar stresses in composite laminates. Int. J. Solids Struct. 26, 331–351.

Yin, W.L., 1994a. Free-edge effects in anisotropic laminates under extension, bending and twisting. Part I: A stress-function-based variational approach. J. Appl. Mech. 61, 410–415.

Yin, W.L., 1994b. Free-edge effects in anisotropic laminates under extension, bending and twisting. Part II: Eigenfunction analysis and the results for symmetric laminates. J. Appl. Mech. 61, 416–421.